

https://doi.org/10.1038/s42003-025-07465-6

Activation of TMEM16E scramblase induces ligand independent growth factor receptor signaling and macropinocytosis for membrane repair



Jung-Eun Kim¹, Woori Ko ®¹, Siwoo Jin², Jin-Nyeong Woo¹, Yuna Jung¹, Inah Bae¹, Han-Kyoung Choe ®¹, Daeha Seo ®², Bertil Hille ®³ & Byung-Chang Suh ®¹ ⊠

The calcium-dependent phospholipid scramblase TMEM16E mediates ion transport and lipid translocation across the plasma membrane. TMEM16E also contributes to protection of membrane structure by facilitating cellular repair signaling. Our research reveals that TMEM16E activation promotes macropinocytosis, essential for maintaining plasma membrane integrity. This scramblase externalizes phosphatidylserine, typically linked to resting growth factor receptors. We demonstrate that TMEM16E can interact with and signal through growth factor receptors, including epidermal growth factor receptor, even without ligands. This interaction stimulates downstream phosphoinositide 3-kinase and facilitates macropinocytosis and internalization of annexin V bound to the membrane, a process sensitive to amiloride inhibition. Although TMEM16E is internalized during this process, it returns to the plasma membrane. TMEM16E- driven macropinocytosis is proposed to restore membrane integrity after perturbation, potentially explaining pathologies in conditions like muscular dystrophies, where TMEM16E functionality is compromised, highlighting its critical role in muscle cell survival.

Mutations of TMEM16E (also known as ANO5), a transmembrane protein within the TMEM16 family, are implicated in human diseases such as muscular dystrophies, including Miyoshi muscular dystrophy 3 (MMD3) and limb-girdle muscular dystrophy 2 L (LGMD2L), and a bone deformation and fragility disorder, gnathodiaphyseal dysplasia (GDD)^{1,2}. Functioning as a non- selective ion channel and a phospholipid scramblase, TMEM16E operates in a Ca²⁺-dependent manner, to facilitate simultaneous transport of ions and phospholipid headgroups via a hydrophilic groove. This concurrent transport is termed the "credit-card" mechanism³. In another "out-of- groove" mechanism the phospholipid scramblase apparently transfers phospholipid headgroups outside the hydrophilic groove without channel activity^{4,5}. TMEM16E scramblase activity significantly impacts membrane dynamics by catalyzing phospholipid transfer across the bilayer, influencing cell-to-cell fusion in muscle progenitor cells (MPCs)².

Plasma membrane integrity, characterized by the asymmetrical distribution of phospholipids, is vital for cell survival, morphology, and interaction with the environment. Phosphatidylserine (PS), a key negatively

charged phospholipid located in the inner leaflet of the plasma membrane, supports the lipid bilayer structure and facilitates essential cellular functions such as signaling, survival, and proliferation⁶. Membrane damage and Ca²⁺ influx disrupt this asymmetry by translocating PS to the outer leaflet, thereby initiating processes like platelet activation and blood coagulation. PS exposure is typically activated by apoptotic signals and plays a crucial role in promoting the recognition and removal of apoptotic cells, where external PS acts as an early warning signal for impending cell death^{7,8}. To counteract this disruption of membrane asymmetry, cells utilize protective membrane repair mechanisms⁹, including macropinocytosis, a clathrin-independent form of endocytosis that involves the non-specific uptake of plasma membrane and extracellular nutrients^{10,11}.

Phospholipid scramblases have traditionally been associated with the induction of cell apoptosis; however, recent studies suggest a new perspective linking them to cellular protection mechanisms. The TMEM16 family member, TMEM16F, has been highlighted for its role in plasma membrane repair via its dual function as a scramblase and ion channel. It is

¹Department of Brain Sciences, Daegu Gyeongbuk Institute of Science and Technology (DGIST), Daegu, 42988, Republic of Korea. ²Department of Physics and Chemistry, Daegu Gyeongbuk Institute of Science and Technology (DGIST), Daegu, 42988, Republic of Korea. ³Department of Neurobiology and Biophysics, University of Washington, Seattle, WA, 98195, USA. ⊠e-mail: bcsuh@dgist.ac.kr

posited that externalization of PS by TMEM16F could signal cellular repair mechanisms to restore membrane integrity ("repair me" or "don't eat me" signals)¹². TMEM16E's association with calcium homeostasis and membrane recovery is also documented in myocytes^{2,13,14}, but precise molecular pathways by which PS exposure facilitates "repair me" signaling remain elusive.

Our study explores how phosphatidylserine (PS) exposure, induced by the TMEM16E scramblase, initiates protective mechanisms. We found that membrane-targeted annexin V (AV), also known as annexin A5, was internalized into the cytoplasm during TMEM16E scramblase activity. This process was halted by amiloride, a macropinocytosis inhibitor¹⁵. Additionally, we discovered that growth factor receptor (GFR) activation was triggered by active TMEM16E scramblase and sustained through interactions with phosphatidylinositol 4,5-bisphosphate [PI(4,5)P₂], leading to the activation of phosphoinositide 3-kinase (PI3K) and the induction of macropinocytosis. These findings highlight the interaction of TMEM16E with GFRs as a pivotal step for ligand-independent GFR activation. Consequently, our research proposes that intracellular Ca²⁺-induced PS exposure could trigger TMEM16E-mediated macropinocytosis, reinstating membrane asymmetry. This molecular mechanism underscores the crucial role of TMEM16E in cell survival by preserving plasma membrane integrity and restoring asymmetry under physiological stress.

Results

Induction of endocytic pathways by 1 µM A23187 in TMEM16E-expressing HEK293T cells

Multiple mechanisms move phospholipids between the leaflets of the plasma membrane. For clarity, when referring to a specific molecular mechanism, we refer to the phospholipid scramblase TMEM16E by name, and when instead, inducing phospholipid scrambling activity experimentally in cells for example by raising cytoplasmic Ca²⁺, we refer to the activity by more generic terms such as "endogenous Ca²⁺-PLS." The endogenous Ca²⁺-PLS activity may depend on several families of phospholipid scramblases¹⁶. To understand the nature of endogenous Ca²⁺-PLS, we compared scrambling activity induced by 1 µM of the Ca²⁺ ionophore A23187 in cells expressing green fluorescent protein (GFP) alone or TMEM16E-GFP. Consistent with the previous studies¹, our confocal experiments revealed that a significant portion of TMEM16E was localized at the plasma membrane (PM), despite its primary expression in the endoplasmic reticulum (ER) (Supplementary Fig. 1). Phospholipid scrambling initiates exposure of PS on the outer leaflet of the plasma membrane, revealed as the binding of extracellular AV to outward-facing PS¹⁷. Application of AV-binding buffer with 1 µM A23187 revealed transfer of PS in cells expressing TMEM16E-GFP but not in cells expressing GFP alone, and it required the inclusion of A23187 (Fig. 1a, b; Supplementary Fig. 2a-c). Using another PS-binding biosensor, GFP-LactC2^{18,19}, we found that the time courses for AV binding to the PM and LactC2 translocation to the cytosol from the PM were very similar (Supplementary Fig. 2d, e), suggesting that the membrane-targeted AV accurately indicates PS exposure under our experimental conditions. Thus, 1 μ M A23187 evoked TMEM16E scramblase activity but not endogenous Ca2+-PLS.

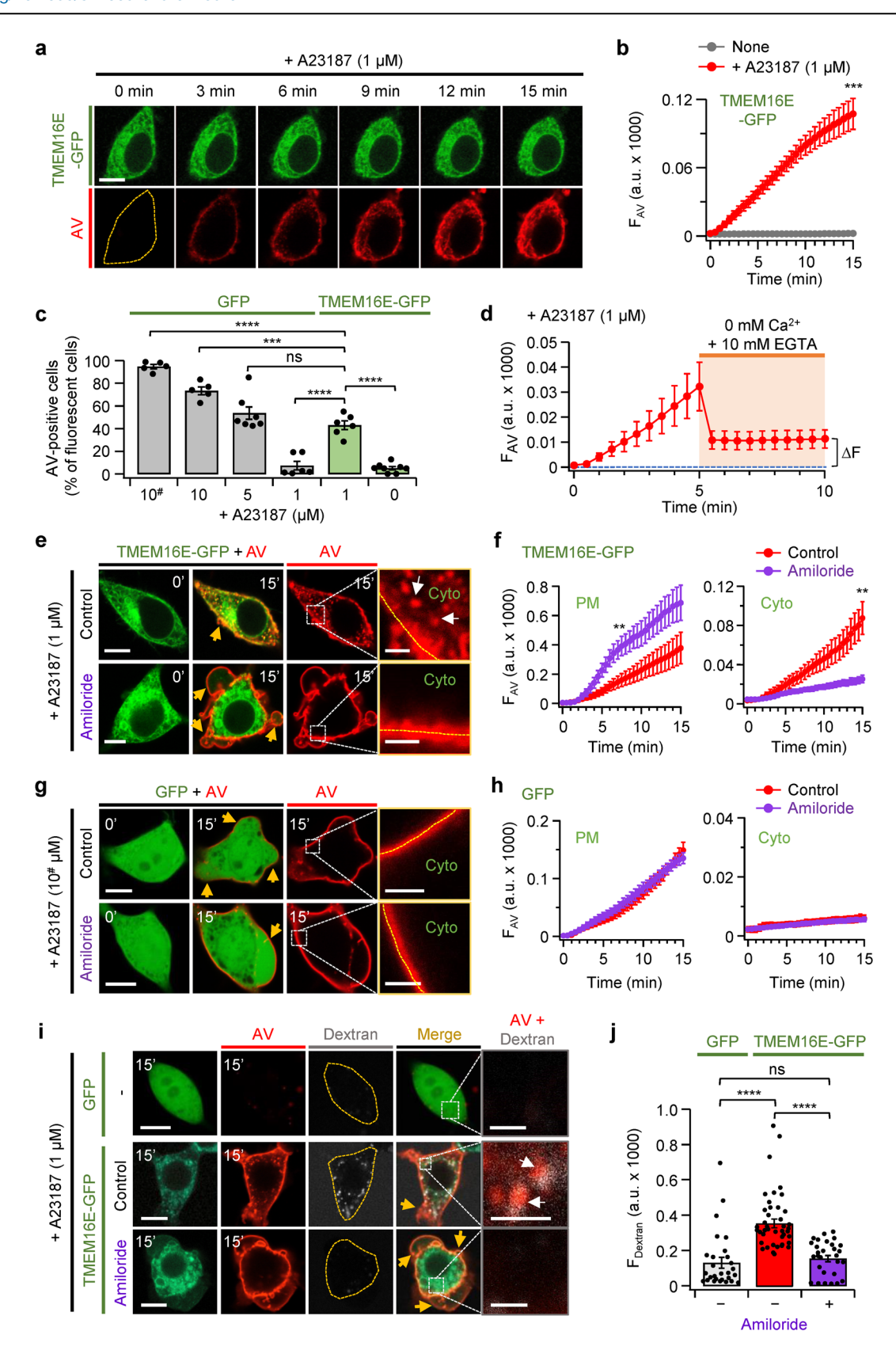
More powerful protocols evoked endogenous Ca^{2+} -PLS. We quantified the percentage of AV-positive cells after Ca^{2+} treatments using confocal microscopy. For example, consider a strong protocol that we designate "10*". In this 10* protocol, cells not expressing TMEM16E were bathed in zero Ca^{2+} extracellular solutions containing 10 μ M A23187 for 5 min to exhaust intracellular calcium stores, followed by application of 2.5 mM Ca^{2+} extracellular solutions containing AV for 15 min to strongly increase calcium entry into the cytoplasm. This led to robust increases in endogenous Ca^{2+} -PLS with up to 95 ± 2% of cells showing AV binding, significantly more than the responses with 10 μ M (73 ± 3%), 5 μ M (54 ± 5%), or 1 μ M (7 ± 4%) A23187 without pretreatment. For comparison, 43 ± 4% of cells expressing TMEM16E responded to 1 μ M A23187 treatment (Fig. 1c), so we considered this response to be TMEM16E specific. Following scramblase induction by our standard protocol, we monitored changes in AV

localization after secondary removal of extracellular calcium. TMEM16E transfected cells were treated as usual with 2.5 mM Ca²⁺ AV-binding buffer containing 1 µM A23187 for up to 5 min, and then the extracellular calcium concentration was reduced to 0 mM Ca2+ with AV-binding buffer containing 10 mM EGTA. Binding of AV to PS involves Ca²⁺-bridges¹⁷, and upon removal of extracellular calcium, the amount of AV bound to cells dropped abruptly (Fig. 1d; Supplementary Fig. 2f). Nevertheless, in the confocal images, a significant amount of AV remained that had been internalized in the cell (Fig. 1e, top), raising the possibility that a specific endocytic pathway had been activated by TMEM16E-dependent scramblase. The TMEM16E-mediated endocytosis was not significantly affected by temperature (Supplementary Fig. 3). Among many possible endocytic pathways²⁰, we hypothesized that macropinocytosis might be responsible. It plays an important role in cell survival by facilitating non-selective internalization of damaged cell membranes²¹. So, we compared internalization of AV in control cells and in cells treated before imaging with 3 mM amiloride, a macropinocytosis blocker¹⁵. Indeed, internalization of AV was almost completely inhibited by amiloride (Fig. 1e, bottom). AV fluorescence intensity in the cytoplasmic region was significantly reduced in cells treated with amiloride (Fig. 1f), whereas AV fluorescence intensity at the plasma membrane was significantly elevated. Apparently, AV that was prevented from entering was building up at the plasma membrane. Additionally, we conducted these experiments in HEK293T clones that stably express TMEM16E via lentivirus transduction. In the stable cell line expressing GFP, the application of 1 µM A23187 did not trigger any scrambling activity (Supplementary Fig. 4). However, in cells stably expressing TMEM16E-GFP, a strong scrambling activity was induced at the plasma membrane (PM), leading to the internalization of membrane- targeted AV into the cytoplasmic region. This internalization was also inhibited by amiloride. These results indicate that the scrambling activity of TMEM16E promotes PS exposure on the cell surface and facilitates macropinocytosis of the membrane, both in stable and transient expression systems. However, when endogenous Ca²⁺-PLS was induced by a 10 µM A23187 pretreatment using the 10[#] protocol in cells expressing only GFP rather than TMEM16E-GFP, AV binding but no internalization was detected (Fig. 1g, h). Apparently, TMEM16E-scramblase but not endogenous Ca²⁺-PLS could induce macropinocytosis.

Activating TMEM16E-dependent scramblase initiated formation of small blebs at the plasma membrane, which were dramatically increased both in size and number within several minutes of treatment with amiloride (Fig. 1e; Supplementary Fig. 5a; Supplementary Movies 1, 2). Perhaps normal blebbing was being dynamically opposed by an ongoing amiloridesensitive macropinocytosis. When endogenous Ca²⁺-PLS was induced by the 10 µM A23187 pretreatment 10[#] protocol in cells expressing only GFP, internalization of AV was not detected (Fig. 1h), and membrane blebbing was enhanced with or without pre-treatment with amiloride (Fig. 1g, large round bulges at arrows; Supplementary Fig. 5b; Supplementary Movies 3, 4). Without TMEM16E, AV binding was not as strong as with TMEM16E although high intracellular Ca²⁺ rise could activate endogenous scrambling and blebbing. Similarly, in cells expressing TMEM16F, the application of A23187 triggered AV binding to the PM, but did not induce AV internalization to the cytoplasm, suggesting that TMEM16F was ineffective in evoking internalization (Supplementary Fig. 5c, d). To confirm that internalization of AV occurred through endocytic pathways, cells were treated before imaging with dextran, an endocytic tracer. Dextran was translocated to the cytoplasmic domain and co-localized with internalized AV when cells expressed TMEM16E. Application of amiloride completely suppressed dextran internalization (Fig. 1i, j). These results indicate that AV internalization was mediated by macropinocytosis during TMEM16Edependent lipid scrambling.

Activation of TMEM16E-dependent scramblase can initiate endocytosis independently of intracellular Ca²⁺

So far, to initiate scramblase activity, we elevated calcium using a Ca²⁺ ionophore. Our next experiments raised calcium via activation of the G



protein-coupled M_1 muscarinic receptor (M_1R). We monitored intracellular Ca^{2+} levels using the Ca^{2+} indicator Fluo-4 in cells with TMEM16E alone or co-expressing M_1R ($+M_1R$). Application of 10 μ M of the muscarinic agonist oxotremorine-M (Oxo-M) did not elevate Ca^{2+} or initiate AV internalization in cells expressing TMEM16E alone, but did elevate Ca^{2+}

and initiate AV internalization in cells co-transfected with M_1R and TMEM16E (Fig. 2a–c). This internalization could be blocked by amiloride (Fig. 2c, d). When Oxo-M was added to cells transfected with M_1R but no TMEM16E (GFP only), there was only minor and non-significant binding of AV to the membrane and no meaningful endocytosis (Supplementary

Fig. 1 | In cells expressing TMEM16E, annexin V (AV) targeted the plasma membrane and some was internalized. a Representative confocal images of TMEM16E and AV after application of 1 µM A23187 to induce scrambling activity in HEK293T cells. Scrambling of membrane PS was revealed by recruitment of AV from AV-binding buffer. The yellow dashed line shows the ROI. Scale bars, 10 µm. b Total AV fluorescence intensity in whole-cell ROIs every 30 s for 15 min without (None) or with 1 μ M A23187 treatment (None, n = 5; + A23187 1 μ M, n = 10). ***P < 0.001, compared with control, determined by Student's t-test. c Percent of AV-positive cells as a function of A23187 concentration in cells expressing GFP $(+ A23187 \ 10^{\dagger} \mu M, n = 5; 10 \mu M, n = 5; 5 \mu M, n = 7; 1 \mu M, n = 6)$ or TMEM16E (+ A23187 1 μ M, n = 6; without A23187, n = 8). The individual data represent the percentage of AV-positive cells over the total cells expressing GFP or TMEM16E of one coverslip. Protocol 10[#] applied zero Ca²⁺ external solution containing 10 μM A23187 for 5 min, and then 2.5 mM Ca2+ external solution with diluted 1:200 AV for 15 min. Analysis was performed by one-way ANOVA followed by Tukey's post-hoc test (GFP 10[#] μM vs TMEM16E 1 μM, ****P < 0.0001; GFP 10 μM vs TMEM16E, ***P = 0.0001; GFP 5 μ M vs TMEM16E 1 μ M, ns = 0.3466; GFP 1 μ M vs TMEM16E $1 \mu M$, ****P < 0.0001; TMEM16E 1 uM A23187 vs without A23187, ****P < 0.0001). **d** Time course of the fluorescence intensity of AV in the whole region of cells expressing TMEM16E. Application of 2.5 mM Ca²⁺ AV binding buffer for 5 min was followed by treatment with 0 mM Ca²⁺ AV binding buffer containing 10 mM EGTA (n = 8). ΔF denotes the residual AV fluorescence intensity in the cytoplasmic region. e Confocal images as application of 1 uM A23187 induced TMEM16E-dependent scramblase (green) and membrane- targeted AV (red)

internalized into the cytoplasm. Inhibition of AV internalization by 3 mM amiloride in DMEM for 15 min. The white arrows show the internalized AV. g Protocol 10# induced endogenous-Ca²⁺-PLS in cells expressing GFP. Cell images of control or after application of 3 mM amiloride. The yellow arrows point to membrane blebbing. The white dashed square box is magnified in the images in the right panel and the yellow dashed lines represent the plasma membrane region. Scale bars, $10\,\mu m$, and magnified images scale bar, 2 µm. f, h AV fluorescence intensity in experiments like those of (e, g). ROIs were selected from the plasma membrane (PM) or cytoplasmic region (Cyto) in cells expressing TMEM16E (\mathbf{f} ; Control, n = 11; Amiloride, n = 6) and GFP-C1 (h; Control, n = 6; Amiloride, n = 5). Compared with the control, determined by Student's t-test (Control PM vs Amiloride PM, **P = 0.0071; Control Cyto vs Amiloride Cyto, **P = 0.0039). i Representative images of cells expressing GFP or TMEM16E-GFP. Cells were treated with 0.3 mg/mL dextran, an endocytic tracer for 2 h in DMEM before imaging. The white arrows indicate colocalized AV and dextran. The yellow dashed lines representing the plasma membrane outline the ROIs. The white dashed square box is magnified in the images in the right panel and the yellow arrows indicate blebs of the plasma membrane. Scale bars, 10 $\mu m,$ and magnified images scale bar, 2 µm. i Analysis of dextran fluorescence intensity at 15 min after treatment of 1 μ M A23187 in cells expressing GFP (Control, n = 28) or TMEM16E (Control, n = 42; Amiloride, n = 29). Analysis was performed by oneway ANOVA followed by Tukey's post-hoc test (GFP Control vs TMEM16E Control, ****P < 0.0001; GFP Control vs TMEM16E Amiloride, ns (not significant) = 0.8143; TMEM16E Control vs TMEM16E Amiloride, ****P< 0.0001). Data are mean ± SEM.

Fig. 6a, b). Thus, M₁R activation could trigger the TMEM16E-requiring, scramblase-driven endocytic pathway.

Are calcium elevations essential for AV internalization by endocytosis? We tried to activate TMEM16E without elevating calcium. In the related Ca²⁺-dependent Cl⁻ channel, TMEM16A, substitution of glutamic acid (E) at position 623 in the third extracellular loop with glutamine (Q) removes a requirement for extracellular protons²². We generated the homologous mutation in TMEM16E(E584Q) (Fig. 2e) and found that this mutant form seemed to have mild constitutive activity, not requiring Ca²⁺ elevation. The lipid scrambling activity of E584Q was further examined with the Ca²⁺independent PS-binding LactC2^{18,19}. We found that GFP-LactC2 was primarily localized at the plasma membrane in cells co-expressing TMEM16E WT, whereas the probe was mainly distributed throughout the cytoplasm in cells co-expressing E584Q, even in the absence of external Ca2+ (Supplementary Fig. 6c, d). These data further support that E584Q can display constitutive scramblase activity in a Ca²⁺-independent manner. Although cellular intracellular calcium was not raised by the mutation (Supplementary Fig. 6e-g), E584Q catalyzed AV internalization with AV-binding buffer lacking 1 µM A23187 (Fig. 2f, g). Consistently, E584Q also triggered the translocation of dextran to the cytoplasm even in the absence of external Ca²⁺ (Supplementary Fig. 6h, i). Furthermore, the application of amiloride completely suppressed dextran internalization and the Ca²⁺-independent AV incorporation. These results suggested that some PS scrambling already had occurred constitutively in the TMEM16E(E584Q) cells before addition of AV and that macropinocytosis does not require a Ca²⁺ elevation when TMEM16E is activated by this mutation. The intracellular Ca²⁺-independence of macropinocytosis was further tested using two variants, TME-M16E(C341Y) and TMEM16E(T498I), which are GDD-related mutants exhibiting scrambling activity even in the absence of Ca^{2+1,23}, Using confocal microscopy, we confirmed that constitutive scrambling activity and internalization of membrane-targeted AV were observed in cells expressing C341Y or T498I without treatment with ionophore, and these phenomena were completely abolished by amiloride treatment (Supplementary Fig. 7). These results support the notion that the two gain-of-function mutants associated with TMEM16E-related muscular dystrophy also induce macropinocytosis in a Ca²⁺-independent manner.

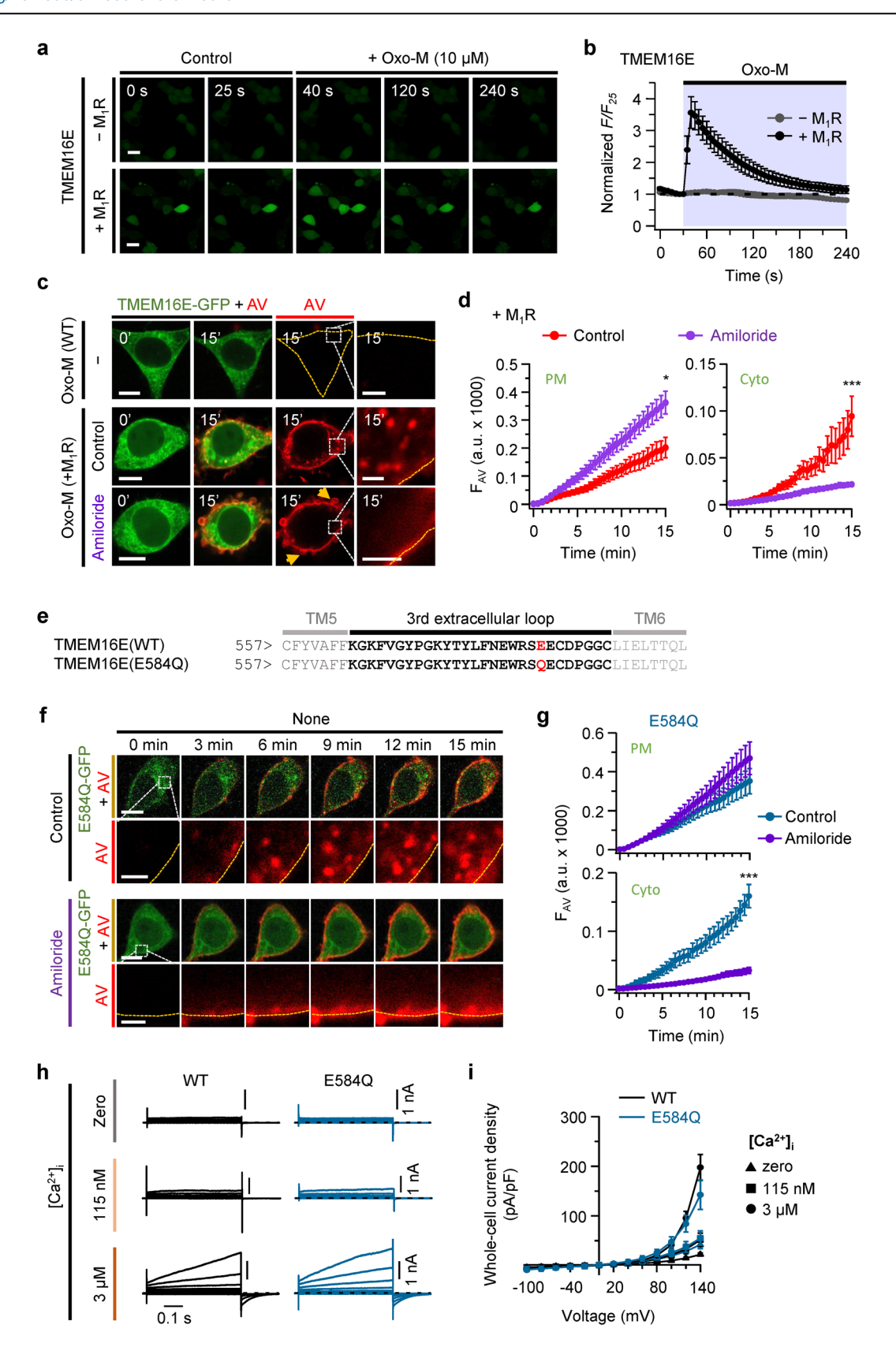
We then compared WT and E584Q TMEM16E as non-selective ion channels. We measured whole-cell ion currents in both forms with and without Ca²⁺ in the pipette solutions. Without pipette Ca²⁺, neither TMEM16E WT nor E584Q exhibited ion currents; however, with 115 nM or 3 µM Ca²⁺ pipette solutions, both showed appreciable currents at high

voltages without significant differences in current density (Fig. 2h, i). Scramblases are traditionally understood to operate via a credit-card-like mechanism, concurrently passing phospholipid headgroups and ions through a hydrophilic groove, but they also can transport phospholipids without ion movements via an out-of-groove mechanism that thins the membrane⁴. We infer that the constitutive activity of E584Q uses such an out-of-groove mechanism, allowing lipid scrambling even when the ion channel is closed.

PI3K participates in activation of macropinocytosis via TMEM16E-dependent scramblase

In our experiments, an amiloride-sensitive endocytic pathway was activated in TMEM16E- expressing cells. As a hypothesis to guide further experiments, we considered the schematic of Fig. 3a, which proposes that downstream of TMEM16E lie GFRs that signal by PI3K to initiate membrane ruffling and by an extended pathway to initiate the fusion and conversion of ruffles into macropinosomes. This schematic was partly inspired by reports of functional complexes of TMEM16A and TMEM16J with EGFR^{24,25}, by reports of activated Rac1/Cdc42 inducing cytoskeletal remodeling^{15,26}, and by other work showing macropinocytosis induced by direct agonist stimulation of GFRs^{27,28}. Our evidence begins with using PI3K inhibitors wortmannin and LY294002. Cells transfected with TMEM16E were pre-treated with 300 nM wortmannin for 1 h or 50 μM LY294002 for 30 min before treatment with A23187 and imaging. Both inhibitors reduced A23187-stimulated AV internalization significantly and favored membrane blebbing (Fig. 3b, c; Supplementary Fig. 8a, b). AV fluorescence on the plasma membrane was not significantly changed with wortmannin treatment, but was significantly increased by LY294002 (Supplementary Fig. 8a). Wortmannin inhibits Rac1-mediated membrane ruffles by inhibiting PLC γ^{29} , but LY294002 inhibits only ruffle fusion³⁰. We also found that the application of the Pak1 inhibitor IPA-3 (20 μM) or the Rac1 inhibitor EHT-1864 (10 µM) nearly completely inhibited the AV internalization, with the Pak1 inhibitor showing a stronger effect (Fig. 3b, d). The findings with these inhibitors support a downstream signaling pathway involving PI3K and PLCy.

We continued our focus on PI3K. This lipid kinase generates phosphatidylinositol 3,4,5-trisphosphate [PI(3,4,5)P₃] in the plasma membrane by phosphorylation of PI(4,5)P₂. Accordingly, we looked for elevations of PI(3,4,5)P₃ in the plasma membrane using as a fluorescent PI(3,4,5)P₃ probe, the pleckstrin homology domain of Bruton's tyrosine kinase tagged with GFP (PH-Btk-GFP). However, since resting HEK293T cells already



had enough plasma membrane PI(3,4,5)P₃ to evoke migration of this sensitive probe to the plasma membrane³¹, it was difficult to check for further increases in PI(3,4,5)P₃ levels induced by TMEM16E-dependent scramblase. Therefore, we first lowered the constitutive activation of GFRs by prestarving transfected HEK293T cells in serum- free medium for 6 hours.

This reduced PI(3,4,5)P $_3$ levels in the cell membrane as evidenced by significant translocation of the PI(3,4,5)P $_3$ probe back to the cytoplasm (Supplementary Fig. 9a, b). Upon application of 1 μ M A23187 to the prestarved cells (Control), we observed significant translocation of PH-Btk-GFP from the cytoplasm to the plasma membrane compared to without

Fig. 2 | Effects of physiological or constitutive activation of TMEM16Edependent scramblase for endocytosis. a Confocal images of Fluo-4 fluorescence representing intracellular Ca²⁺ levels in cells expressing TMEM16E alone (- M₁R) and co-expressing TMEM16E and M_1R ($+M_1R$) treated with 10 μ M Oxo-M. Scale bars, 20 μm. b Normalized fluorescence time course representing intracellular Ca2+ levels every 5 s (TMEM16E alone, n = 49; TMEM16E + M₁R, n = 23). c Confocal images of TMEM16A (green) and AV (red) during 10 µM Oxo-M induced scrambling activity in cells expressing TMEM16E alone (- M1R) or co-expressing TMEM16E and M_1R (+ M_1R). Amiloride (3 mM) was used to block internalization. The yellow dashed line traces the plasma membrane and the outlined yellow dashed line shows the cell area. The white dashed square box is magnified in the images in the right panel and the yellow arrows indicate blebs on the plasma membrane. Scale bars, 10 μm, and magnified images scale bar, 2 μm. d, g Timedependent growth of AV fluorescence intensity in cells co-expressing TMEM16E and M_1R (d; Control, n = 10; Amiloride, n = 11) or expressing E584Q (g; Control, n = 13; Amiloride, n = 13). Analyzed ROIs selected the plasma membrane (PM) and a region of cytoplasm (Cyto). Compared with control, determined by Student's t-test

(**d**, Control PM vs Amiloride PM, *P = 0.0199; **d**, Control Cyto vs Amiloride Cyto, ***P < 0.001; **g** Control Cyto vs Amiloride Cyto, ***P < 0.001). **e** Sequence alignment of TMEM16E WT and E584Q. The black line marks the 3rd extracellular loop of TMEM16E. The negatively charged glutamate at E584 indicated in red was selectively mutated to glutamine. f Representative images of scrambling activity in cells expressing TMEM16E E584Q treated with AV-binding buffer without A23187. Cells were untreated with control or treated with 3 mM amiloride before imaging. The yellow dashed line shows the plasma membrane area and the white dashed square box is magnified in the images in the bottom panel. Scale bars, $10 \, \mu m$, and magnified images scale bar, $2 \mu m$. h Whole-cell currents elicited by voltage steps from -100 to +140 mV in 20 mV intervals in cells expressing WT and E584Q TMEM16E with the zero $[Ca2+]_i$, 115 nM $[Ca^{2+}]_i$, or 3 μ M $[Ca^{2+}]_i$ pipette solution. The holding potential was -60 mV and the black dashed line shows zero current. i Analysis of current density versus voltage relationships for WT and E584Q TMEM16E with zero $[Ca^{2+}]_i$ (WT, n = 8; E584Q, n = 6), 115 nM $[Ca^{2+}]_i$ (WT, n = 8; E584Q, n = 7), or 3 µM [Ca²⁺]_i (WT, n = 11; E584Q, n = 6) intracellular pipette solution. Data are mean ± SEM.

A23187 (none) (Fig. 3c, e). Thus, scramblase activation increased PI(3,4,5) P₃ in the membrane. Inhibition of PI3K with 300 nM wortmannin abrogated probe translocation. Additionally, we observed that membrane blebs actively formed on the plasma membrane and were internalized by macropinocytosis in control cells, whereas the blebs formed but continuously increased in size in the wortmannin-treated cells (Fig. 3c; Supplementary Fig. 9c; Supplementary Movies 5, 6). It is known that PI3K is important for inducing membrane ruffles to form a macropinocytic cup and macropinosomes via ruffle priming³². Correspondingly, we observed in control cells that the size of membrane blebs was regulated through TMEM16Emediated macropinocytosis, but in wortmannin-treated cells PI3K activity blocked, membrane bleb size continued to increase. Additionally, endogenous Ca²⁺-PLS in cells expressing mCherry vector did not increase PI3K activity and induced membrane blebs regardless of wortmannin (Supplementary Fig. 9d, e), demonstrating that membrane blebs depended on scramblase activity. In summary, we showed that TMEM16E-dependent scramblase triggered macropinocytosis by activating PI3K and PI(3,4,5)P₃ levels.

Ligand-independent GFR activation by TMEM16E through scrambling and $PI(4,5)P_2$

How does TMEM16E-dependent scramblase raise PI3K activity? Typical growth factor receptors (GFRs) like epidermal growth factor receptor (EGFR), platelet-derived growth factor receptor (PDGFR), and colonystimulating factor-1 (CSF-1), key inducers of macropinocytosis^{27,28}, are modulated by plasma membrane phospholipids. In the absence of receptor ligand, PS of the cytoplasmic leaflet stabilizes EGFR in its inactive state by binding to basic residues in the intracellular juxtamembrane domainautoinhibition³³. Binding of EGFR ligand triggers structural shifts, prompting juxtamembrane basic residues to link instead with PI(4,5)P₂ on the inner leaflet³³. This informs our schematic for GFR activation via TMEM16E. In cells with TMEM16E, the GFR would be interacting electrostatically with inner-leaflet PS headgroups prior to 1 µM A23187 exposure (Fig. 4a, left). When activated, TMEM16E scramblase flips PS to the extracellular leaflet, removing it from receptors, which make new interactions with inner-leaflet PI(4,5)P2 and switch to their active configuration (Fig. 4a, right). This would be a second role for PI(4,5)P₂ in this pathway, the other one being PI(4,5)P2 as a precursor of PI(3,4,5)P3. To test for involvement of PI(4,5)P2 in scramblase-stimulated macropinocytosis, we used a rapamycin- induced translocation system to deplete PI(4,5)P₂. The depletion system uses fusion proteins of mRFP-FKBP (RF) linked in tandem to two lipid phosphatases: Sac1 4-phosphatase and INPP5E 5-phosphatase³⁴. RF-PJ (pseudojanin) contains active versions of Sac1 and INPP5E, whereas the first control construct, RF-Dead, contains inactive mutants of Sac1 and INPP5E, and the second control construct RF contains only the active 4-phosphatase Sac1 (Supplementary Fig. 10a). Applying rapamycin recruits these FKBP-containing cytoplasmic fusion proteins to couple with Lyn₁₁-

FRB (LDR) at the plasma membrane. In cells expressing RF constructs and the PH domain from PLC δ 1 (PH-PLC δ 1), a PI(4,5)P₂ sensor, we confirmed that translocation of RF-PJ via rapamycin depleted PI(4,5)P₂ at the membrane, whereas RF-Dead and RF-Sac1 did not (Supplementary Fig. 10b, c). When PI(4,5)P₂ was depleted, we observed no AV internalization during scrambling (Fig. 4b, c). Thus, PI(4,5)P₂ is essential for initiating macropinocytosis by TMEM16E scramblase.

Our schematic (Fig. 3a) suggests that GFRs participate in the TMEM16E signaling pathway. As a first step, we used specific inhibitors for EGFR and PDGFR. Afatinib, is an irreversible covalent EGFR inhibitor³⁵, and imatinib, an allosteric PDGFR inhibitor³⁶ (see Fig. 5a). In TMEM16Eexpressing cells, treatment with 1 µM afatinib completely suppressed A23187-induced AV uptake, whereas 20 µM imatinib reduced it only modestly (Fig. 5b, c). Similarly, the two inhibitors were active in cells expressing the E584Q TMEM16E mutant without 1 µM A23187 treatment (Supplementary Fig. 11). These findings suggest that GFR activation is an obligate step in TMEM16E scramblase-induced macropinocytosis, with EGFR being more efficacious than PDGFR in HEK293T cells. A coimmunoprecipitation assay showed that overexpressed EGFR and PDGFR form molecular complexes with TMEM16E (Fig. 5d), and RT-PCR monitoring of endogenous EGFR and PDGFR expression showed that EGFR was about twice as abundant as PDGFR in HEK293T cells (Fig. 5e). Thus, both EGFR and PDGFR can couple with TMEM16E equally, but EGFR is the predominant coupling intermediate for macropinocytosis because it is more abundant in HEK293T cell system. In co-immunoprecipitation assays, we also found that TMEM16F did not couple with EGFR, while TMEM16E and E584Q formed complexes with the receptors (Fig. 5f, g). These results suggest that macropinocytosis was specifically mediated by TMEM16E scramblase. Finally, we confirmed that the interactions of EGFR and PDGFR with TMEM16E was specific, as there was no coupling between M₁R and TMEM16E (Fig. 5h).

TMEM16E internalization and membrane integrity preservation via macropinocytosis during scrambling activity

We asked whether membrane TMEM16E was internalized by AV-targeted macropinocytosis during scramblase activity. The answer was yes. Using total internal reflection fluorescence (TIRF) microscopy to illuminate just the plasma membrane footprint with an evanescent wave from totally reflected laser light, we tracked TMEM16E-GFP and AV-Alexa-Fluor-568 simultaneously at the cell surface. In resting cells, TMEM16E-GFP remained steady at the membrane (Fig. 6a, c, top). Upon addition of 1 μ M A23187, labeled AV accumulated at the cell surface, but TMEM16E-GFP fluorescence there declined transiently over 7 min and then gradually recovered, even overshooting (Fig. 6a, bottom, and b). Amiloride application halted the initial TMEM16E-GFP decline and instead permitted marked augmentation of TMEM16E-GFP at the membrane after a few minutes (Fig. 6c, bottom, and d). TMEM16E reportedly clusters at plasma

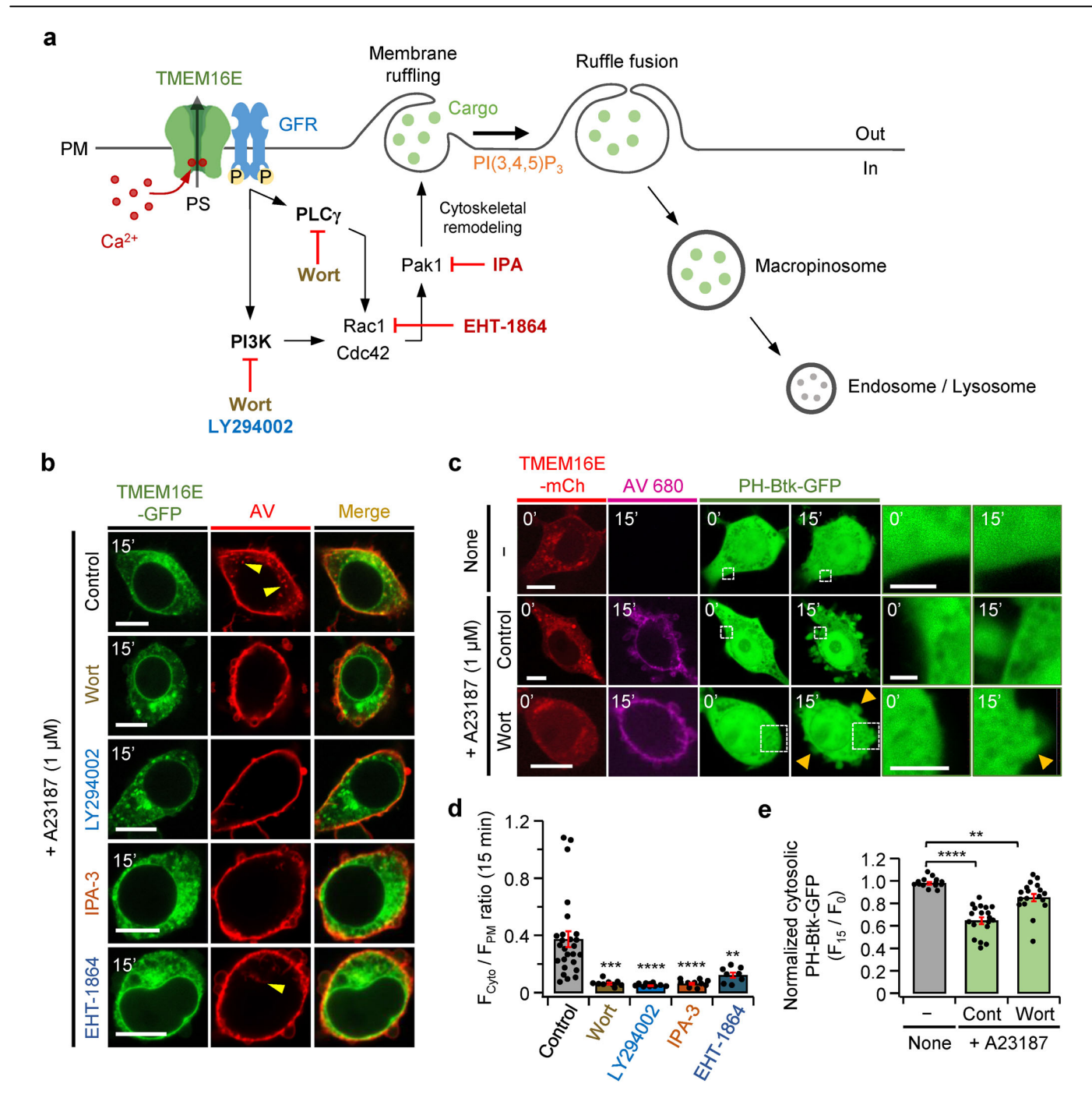


Fig. 3 | PI3K-mediated signaling pathway participates in activation of macropinocytosis via TMEM16E-dependent scramblase. a Schematic hypothesis of signaling downstream of TMEM16E to macropinocytosis. Activation of TMEM16E-dependent scramblase initiates macropinocytosis via growth factor receptors (GFR). GFRs activate PI3K and induce membrane ruffling through Pak1. The membrane ruffles are fused through cytoskeletal remodeling by PI(3,4,5)P₃. The fused membrane enters into the cells as macropinosome vesicles. The images and every material element by the authors using Microsoft Office PowerPoint 365 (Microsoft). b Representative confocal images of 1 μ M A23187-induced scrambling activity in TMEM16E-expressing cells (green) without (Control) or with 300 nM wortmannin (Wort) for 1 h (middle), 50 μ M LY294002 for 30 min, 20 μ M IPA-3 for 15 min, or 10 μ M EHT-1864 for 15 min in medium before imaging. The yellow arrows indicate internalized AV. Scale bars, 10 μ m. c, Representative images of cells co-expressing the PI(3,4,5)P₃ marker PH-Btk-GFP (green) and TMEM16E-

mCherry (red) before and after AV 680 addition (magenta). Without A23187 (None), application of 1 μ M-A23187 (Cont), and after pretreatment with 300 nM wortmannin before imaging and application of 1 μ M A23187 (Wort). Cells were starved in DMEM for 6 h before imaging. The white dashed square box is magnified in the images in the right panel. Scale bars, 10 μ m, and magnified images scale bar, 2 μ m. **d** The ratio of cytoplasmic region (Cyto) and plasma membrane (PM) AV fluorescence intensity ($F_{\rm Cyto}/F_{\rm PM}$ ratio) 15 min after addition of A23187 (Control, n=26; Wort, n=9; LY294002, n=12; IPA-3, n=10; EHT-1864, n=8). Analysis was performed by one-way ANOVA followed by Dunnett's post-hoc test (Compared to control, Wort, ***P < 0.0002; LY294002, ****P < 0.0001; IPA-3, ****P < 0.0001; EHT-1864, **P = 0.0046). **e** Normalized F_{15}/F_0 ratio before and after addition of AV-binding buffer (None, n=14; Cont, n=19; Wort, n=18). Analysis was performed by one-way ANOVA followed by Dunnett's post-hoc test (Compared to None, Cont, ****P < 0.0001; Wort, **P = 0.0072). Data are mean \pm SEM.

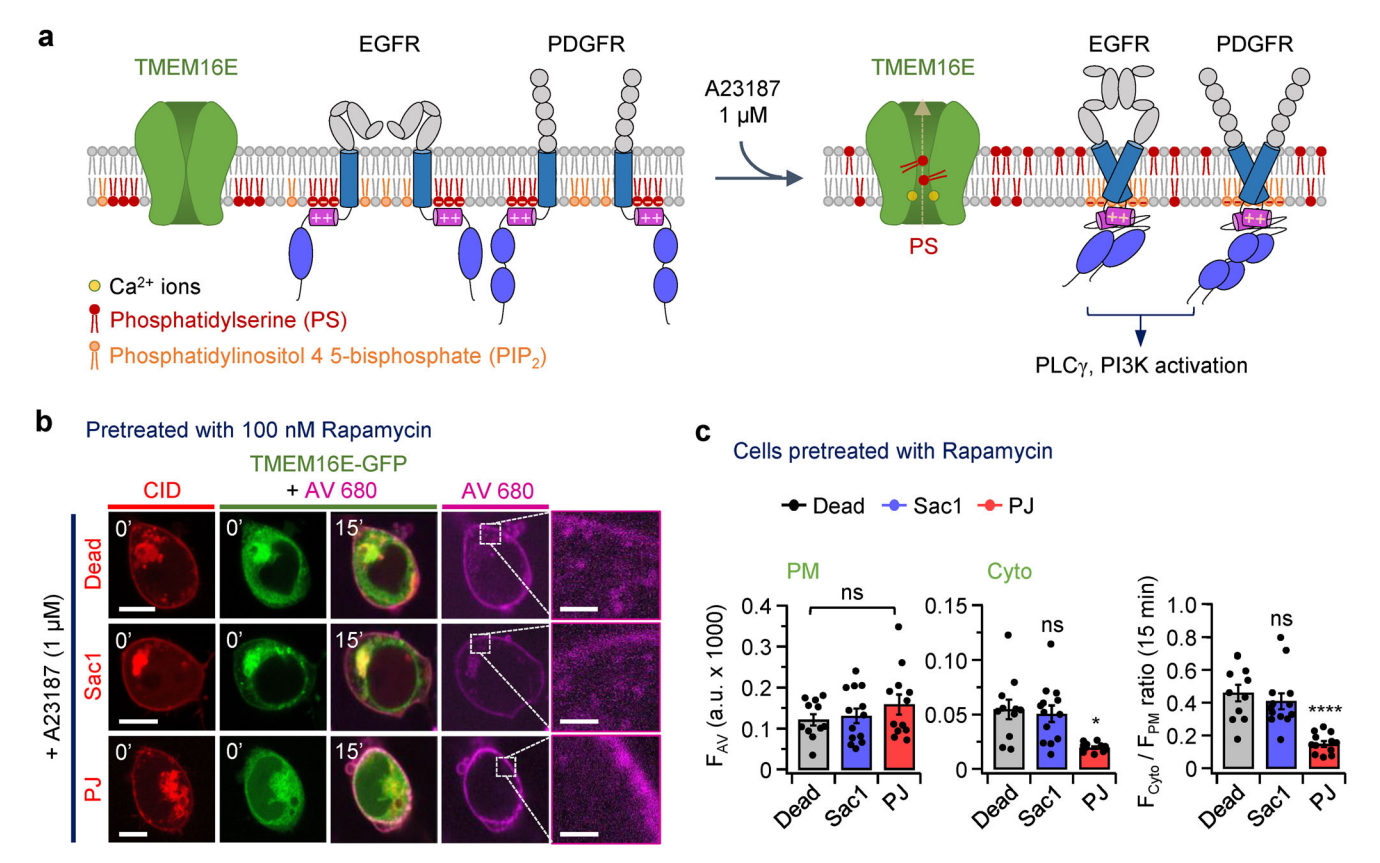


Fig. 4 | TMEM16E-dependent scramblase induces macropinocytosis by activating GFRs and requires PI(4,5)P₂. a Schematic of phospholipid rearrangement by TMEM16E-dependent scramblase and conformational changes of GFRs (EGFR and PDGFR). GFRs consist of an extracellular domain (gray), transmembrane domain (blue), juxtamembrane domain (magenta), and tyrosine kinase domain (purple). Positively charged amino acids of the juxtamembrane domain interact with negatively charged phosphatidylserine (PS) in inactive GFRs. Treatment with A23187 induces TMEM16E-dependent scramblase. The interaction between the juxtamembrane domain and PS is broken, and the juxtamembrane region dimerizes and is converted to an active form by clustering with negatively charged PI(4,5)P₂. Activation of GFRs induces macropinocytosis. The images and every material element by the authors using Microsoft Office PowerPoint 365 (Microsoft).

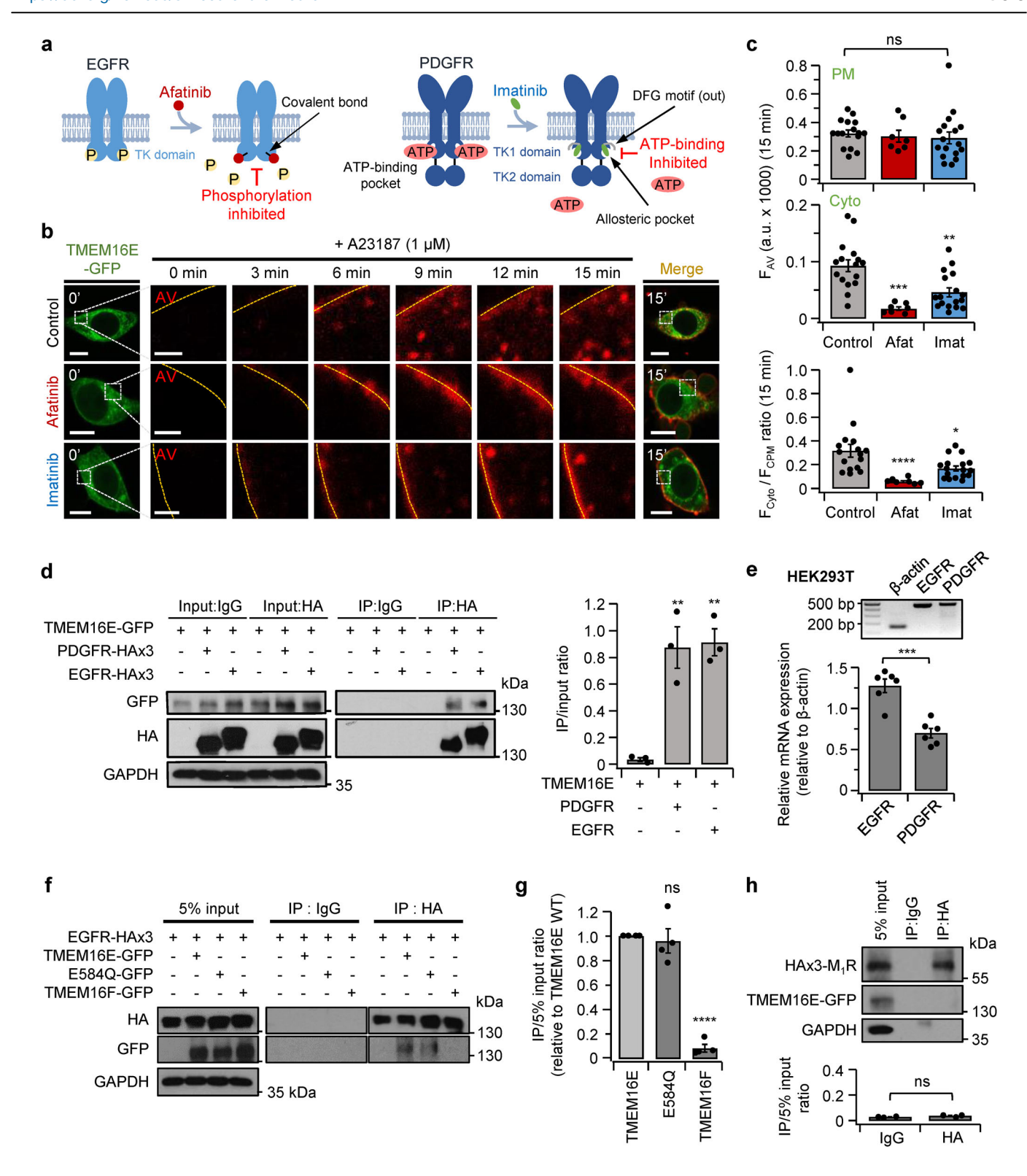
b Representative images of 1 μ M A23187-induced scrambling in cells expressing RF-Dead, RF-Sac1, or RF-PJ with TMEM16E. Cells were treated with 100 nM rapamycin for 10 min in DMEM before imaging. The white dashed square box is magnified in the images in the right panel. Scale bars, 10 μ m, and magnified images scale bar, 2 μ m. **c** Analysis of AV fluorescence intensity at 15 min (RF-Dead, n=11; RF-Sac1, n=13; RF-PJ, n=12). ROIs selected plasma membrane (PM), and cytoplasmic regions (Cyto). The ratio of the cytoplasmic region to the plasma membrane (F_{Cyto}/F_{PM} ratio) was calculated. Analysis was performed by one-way ANOVA followed by Dunnett's post-hoc test (Compared to Dead, PM Sac1, n=0.9218; PM PJ, n=0.3227; Cyto Sac1, n=0.844; Cyto PJ, *P=0.0345; F_{Cyto}/F_{PM} ratio Sac1, n=0.9936; F_{Cyto}/F_{PM} ratio PJ, *****P<0.0001). Data are mean \pm SEM.

membrane damage sites to preserve integrity when the ER fragments from sustained intracellular Ca^{2+} rise due to calcium ionophore ¹⁴. We infer that the increase in late TMEM16E-GFP intensity represents net translocations from the endoplasmic reticulum to the plasma membrane in response to the disruption of membrane asymmetry caused by scrambling activity induced by 1 μ M A23187.

Does TMEM16E-driven macropinocytosis serve as a secondary repair mechanism to clear unwanted exposed PS that was transferred out by its scramblase activity? We considered the formation of blebs as an indicator of compromised membrane with excessive exposed PS. We looked for alterations of cellular morphology by scoring blebbing with and without A23187 in bright field microscopy, comparing cells expressing TMEM16E WT, E584Q, or only GFP in AV- binding buffer (Fig. 6e, f; Supplementary Figs. 12, 13). In the TMEM16E cells, the level of blebbing was low without A23187 ($12 \pm 1\%$ of cells had blebs for control; $13 \pm 1\%$ for amiloride) (Fig. 6e, left, f). Small-sized membrane blebs formed after 1 µM A23187 (63 \pm 4%), and larger and more vigorous blebbing (96 \pm 3%) and significant morphological changes occurred in cells also treated with amiloride for 15 min (Fig. 6e, middle, f). This implies that the TMEM16E- induced macropinocytosis removed blebbing membranes, advancing membrane repair. To assess whether scramblase action itself promotes membrane blebbing even without concomitant intracellular Ca²⁺ increase, we examined blebbing in cells expressing the E584Q mutant or only GFP. In E584Q cells without A23187, blebbing was low (12 \pm 2%) but became remarkably increased with amiloride to block macropinocytosis (79 \pm 2%) (Fig. 6e, right, f; Supplementary Fig. 12; Supplementary Movies 7, 8). In GFP cells, blebbing was low without A23187 (7 \pm 1%) or with 1 μ M A23187 (control, 6 \pm 1%; amiloride, 9 \pm 1%) but developed dramatically with the 10 $^{\sharp}$ protocol (control, 97 \pm 1%; amiloride, 97 \pm 1%) regardless of amiloride (Supplementary Fig. 13). These data implied that blebbing was triggered by intracellular Ca $^{2+}$ rise and that the size or number of blebs increased in proportion to the relative strength of scrambling activity compared to macropinocytosis.

Granule cell TMEM16E: regulating membrane integrity through macropinocytosis

TMEM16E encodes a 913 amino-acid protein that is highly expressed in skeletal muscle, bone, and cardiac muscle¹, and mutations are implicated in several muscle and bone diseases. Brain expression is known for TMEM16A and TMEM16B³⁷, but is not known for TMEM16E. Through RT-PCR, we found expression of TMEM16E in cultured cerebellar granule cells (Fig. 7a, left). Among the TMEM16 family tested, only TMEM16E was endogenously expressed in granule cells together with significant co-expression of EGFR and PDGFR (Fig. 7a, right). However, TMEM16F was not detected in the isolated granule cells, while it was found in the entire cerebellum, as well as in the lungs, heart, and muscles in Sprague-Dawley rat (Supplementary Fig. 14). This suggests that TMEM16E is endogenously expressed in the



granule cell layer, while TMEM16F is primarily localized to other cell layers of the cerebellum.

We then examined scramblase activity in granule cells. First, we applied $5\,\mu M$ A23187 and AV-binding buffer with confocal microscopy. The cells exhibited scramblase-induced membrane ruffling and subsequent partial AV internalization (Fig. 7b, top). Amiloride treatment blocked AV internalization and promoted membrane blebbing (Fig. 7b, bottom). AV uptake during scramblase activity was reduced by the receptor tyrosine kinase inhibitors afatinib and imatinib, confirming macropinocytosis via receptor

tyrosine kinase activation, predominantly through EGFR (Fig. 7c, d; Supplementary Fig. 15a). We further tested whether physiological perturbation could evoke TMEM16E-dependent macropinocytosis in granule cells. Both depolarizing the neurons with 30 mM KCl to activate voltage-dependent Ca²⁺ channels and treating with 5 μ M A23187 raised intracellular calcium levels (Fig. 7e; Supplementary Fig. 15b). The KCl application triggered scramblase activity and robust AV cytoplasmic internalization inhibited by amiloride (Fig. 7f, g). We tried applying 100 μ M ATP, but neither intracellular Ca²⁺ rise nor scramblase activity was induced by ATP (Fig. 7e;

Fig. 5 | Direct interaction between TMEM16E and GFR was critical for macropinocytosis. a Schematic diagram of the action of inhibitors on EGFR and PDGFR. Afatinib inhibits phosphorylation by covalent binding to C797 located in the tyrosine kinase (TK) domain of EGFR. Imatinib binds to the ATP allosteric pocket and blocks the binding of ATP. The images and every material element by the authors using Microsoft Office PowerPoint 365 (Microsoft). b Representative images of TMEM16E-dependent scramblase calculated as AV fluorescence in the plasma membrane (PM) over that in cytoplasm (Cyto) for control, after application of 1 µM afatinib for 1 h, and after 20 µM imatinib for 1 h in DMEM. The yellow dashed line indicates the plasma membrane region and the white dashed square box is magnified in the images in the right panel. Scale bars, 10 μm, and magnified images scale bar, 2 μm. c AV fluorescence intensity 15 min after induction of scramblase in cells treated with GFR inhibitors (Control, n = 16; Afatinib (afat), n = 7; Imatinib (Imat), n = 17). The ratio of the cytoplasmic region (Cyto) to the plasma membrane (PM) was calculated. Analysis was performed by one-way ANOVA followed by Dunnett's post-hoc test (Compared to Control, PM Afat, ns = 0.9189; PM Imat, ns = 0.5111; Cyto Afat, ***P = 0.0002; Cyto Imat, **P = 0.0063; $F_{\text{Cyto}}/F_{\text{PM}}$ ratio Afat, ****P < 0.0001; $F_{\text{Cyto}}/F_{\text{PM}}$ ratio Imat, *P = 0.0392). **d** Protein gels of co-immunoprecipitates performed with anti-HA or IgG in cells expressing TMEM16E-GFP, PDGFR-Hax3, and EGFR-Hax3. The input represents 5% of the lysate used for immunoprecipitation (IP) (n = 3). The result of co-immunoprecipitation with

anti-HA, TMEM16E- GFP was detected with PDGFR-HAx3 and EGFR-HAx3. The summary histogram indicates an interaction of PDGFRxHA3 and EGFR-HAx3 with TMEM16E-GFP. Analysis was performed by one-way ANOVA followed by Dunnett's post-hoc test (Compared to only cells expressing TMEM16E, with PDGFR, **P = 0.0026; with EGFR, **P = 0.0021). e RT-PCR determined the endogenous expression levels of EGFR and PDGFR in HEK293T cells (n = 6). ***P < 0.001, compared with control, analyzed by Student's t-test. f Protein gels of co-immunoprecipitates performed with anti-HA or IgG in cells expressing EGFR-HAx3, TMEM16E-GFP, E584Q-GFP, and TMEM16F-GFP. g Analysis of co-immunoprecipitation with anti-HA and TMEM16E-GFP, E584Q-GFP, and TMEM16F-GFP. The summary shows that EGFR-HAx3 interacts with TMEM16E and E584Q, but not TMEM16F (n = 4). Analysis was performed by one-way ANOVA followed by Dunnett's post-hoc test (Compared to cells expressing EGFR-HAx3 with TMEM16E WT, with E584Q, ns = 0.8639; with TMEM16F, ****P < 0.0001). **h** Protein gels of co- immunoprecipitates performed with anti-HA or IgG in cells expressing TMEM16E-GFP and HAx3-M1R. Coimmunoprecipitation with anti-HA was detected only with HAx3-M1R, but not with TMEM16E-GFP (n = 3). Analysis of the interaction between TMEM16E-GFP with $HAx3-M_1R$. ns = 0.2040, when compared with IgG, analyzed by Student's t-test. Data are mean \pm SEM.

Supplementary Fig. 15c, d). Finally, we investigated the effects of TMEM16E knockdown on the scrambling activity of granule cells using shRNA targeting TMEM16E. We overexpressed pAAV-hSyn-EGFP or pAAV-U6-TMEM16E-shRNA-hSyn-EGFP in primary-cultured granule cells on DIV 4 from Sprague-Dawley rats aged P5 to P6, and measured the scrambling activity and internalization of the AV. As a result, granule cells expressing EGFP only exhibited normal scrambling activity, whereas those expressing rat TMEM16E-shRNA did not (Supplementary Fig. 16). Together, these data suggest that neurons, similar to HEK293T cells, may protect their membrane integrity through TMEM16E-mediated macropinocytosis.

Discussion

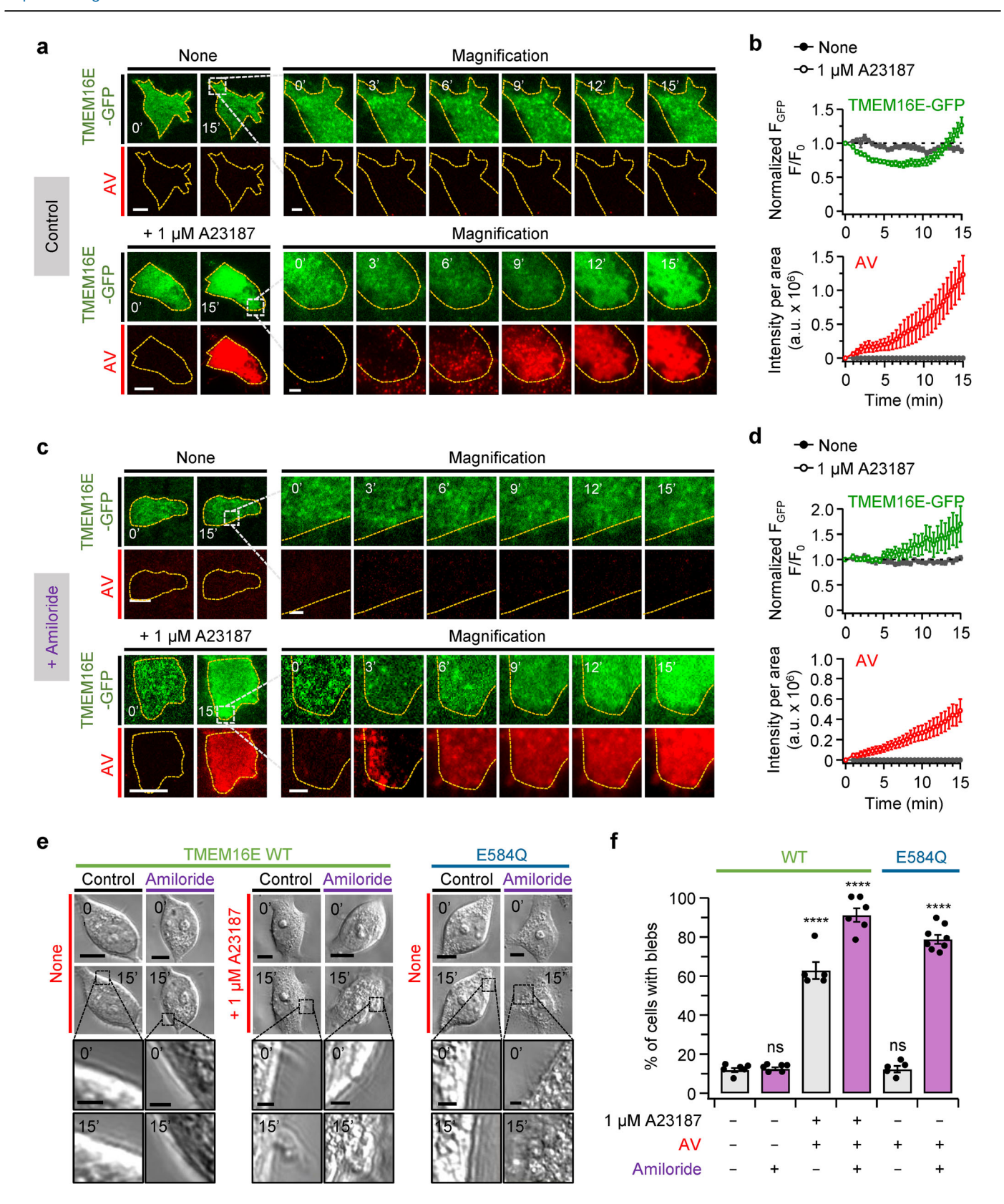
Many studies demonstrate that TMEM16E and TMEM16F are pivotal for plasma membrane repair^{12,13}; however, the molecular connection between scramblase activity and membrane integrity remained elusive. We presented a TMEM16E-mediated mechanism (Fig. 3a) supported by evidence for a need for PI(4,5)P₂, PI(3,4,5)P₃, and GFRs, direct binding of inactive GFR dimers bind to negatively charged PS in the intracellular leaflet³³. In our work, upon activation of G protein-coupled receptors or application of A23187, intracellular calcium elevation activated TMEM16E scramblase with PS translocation to the extracellular membrane leaflet and stimulation of a GFR pathway (Fig. 8, top and middle). This resulted in PI3K- and PI(3,4,5)P₃-driven macropinosome formation through membrane ruffling and fusion, internalizing TMEM16E, GFRs, AV, and presumably the membranes with flipped PS. We presume that macropinosomes eventually merged with lysosomes, degrading GFRs and AV, but gradually cell surface TMEM16E was restored. Since we observed TMEM16E actually overshooting its previous local concentration, likely a new pool of TMEM16E molecules was being recruited to the surface as well as possible recycling of the internalized molecules (Fig. 8, bottom).

Membrane that is damaged by pore-forming agents such as listeriolysin O (LLO)¹², perforin³⁸, or pore-forming proteins³⁹ is rapidly repaired through endocytosis⁴⁰ or exocytosis¹² using intracellular calcium⁴⁰, annexin proteins¹³, and actin cytoskeletal remodeling⁴⁰. Plasma membrane repair systems are critical for maintaining cell homeostasis and ensuring cell survival; for example, they increase neuronal regeneration by restoring the physical barrier that protects cells from deleterious external agents^{41,42}. Plasma membrane repair systems are divided into two stages: an initial process reseals the damaged membrane after injury, and a restructuring process restores membrane homeostasis. The molecular mechanisms of the initial repair process are well studied, but the restructuring process is less understood. It is reported that restructuring mediated by LC3-associated macropinocytosis removes damaged material and restores membrane integrity²¹. During the initial plasma membrane repair, TMEM16E seals the

damaged membrane at the injury site by forming a "repair cap" that includes intracellular annexin I, II, V, and VI proteins¹³. Expression of TMEM16E is essential for initial repair of membrane punctures, and its scrambling activity increases the accumulation of annexin II, but a scrambling-defective mutant still can promote initial repair¹³. Our data showed that the TMEM16E-dependent scramblase removed compromised membrane by activating macropinocytosis. The initial stage of the plasma membrane repair system normally operates in a Ca²⁺-dependent manner^{40,41}, but we found that macropinocytosis could be activated in a Ca²⁺-independent manner with an appropriately mutated TMEM16E scramblase (Fig. 1d; Supplementary Fig. 2d; Fig. 2f, g) and that, once TMEM16E is activated, removal of damaged plasma membrane can proceed without Ca²⁺ elevation. It has been reported that phospholipid scramblase TMEM16F repairs damaged membranes via exocytosis¹². In contrast, we have emphasized the internalization of AVs, TMEM16E, and dextran during scrambling activity in cells expressing TMEM16E, suggesting that TMEM16E might repair damaged membranes through endocytosis.

In cells expressing only GFP, activating endogenous Ca²⁺-PLS exposes PS without triggering macropinocytosis—different from the effects with TMEM16E. We inquired how expressing TMEM16E permits macropinocytosis in a process that requires active GFRs. Our experiments demonstrated that macropinocytosis can be activated by constitutive scrambling activity without the need for added growth factors (Fig. 2; Supplementary Fig. 7). Co- immunoprecipitation showed direct GFR-TMEM16E interaction (Fig. 5d), as previously reported for TMEM16A and TMEM16J where interactions with the juxtamembrane domain of EGFR enhance EGFR protein levels and cancer cell proliferation^{24,25}. We found that TMEM16E- dependent scramblase raised PI(3,4,5)P₃ levels at the plasma membrane by activating GFRs. EGFR and phospholipid scramblase 1 (PLSCR1) are abundant in plasma membrane lipid rafts⁴³; PLSCR1 regulates EGFR interactions and lipid raft composition/stability⁴⁴. Disrupted lipid rafts can activate ligand-independent EGFR clustering⁴⁵. We speculate that TMEM16E-dependent scramblase activity dislodges GFRs from lipid rafts by destabilizing them and induces macropinocytosis by stabilizing ligand-independent GFR activation.

Approximately 50% of receptor tyrosine kinases including EGFR and PDGFR internalize via macropinocytosis upon growth factor binding^{44,46}. We observed co-internalization of TMEM16E, AVs, and GFRs during scramblase activity via TIRF microscopy. Prior studies reported TMEM16E accumulation at injury sites for membrane repair upon calcium influx due to injury¹⁴. Our TIRF microscopy revealed TMEM16E internalization via macropinocytosis with AVs and restoration of TMEM16E at the plasma membrane, while intracellular AV accumulation persisted (Fig. 6a–d). Likely after internalization within macropinosomes, GFRs underwent



lysosomal degradation whereas TMEM16E may have been preserved and recycled to the plasma membrane. PLSCR1 is also recycled to the plasma membrane after internalizing with EGFR through endocytosis⁴⁴.

In humans, TMEM16E is ubiquitously expressed, with high expression in brain, heart, thyroid, and especially skeletal muscles. TMEM16E $\,$

mutations are linked to skeletal muscular dystrophies, including MMD3 and LGMD2L, and the bone dysplasia GDD^{1,47}. Their impact on other tissues remains less explored. Our research highlighted TMEM16E's scramblase activity in cerebellar granule cells (Fig. 7; Supplementary Fig. 15). These cells, which represent over 99% of cerebellar neurons, are integral to

Fig. 6 | Changes in TMEM16E localization and membrane integrity during macropinocytosis. a, c Representative TIRF images of membrane-localized TMEM16E in cells treated with only Ringer's solution or AV-binding buffer containing 1 μ M A23187. Cells are untreated (a) or treated with 3 mM amiloride for 15 min (c) before imaging. The yellow dashed lines represent plasma membrane area. The white dashed square boxes represent ROIs for the magnified view of the images in the right panels. Scale bars, 10 μ m and magnified images scale bar, 2 μ m. b, d Fluorescence intensity at the plasma membrane versus time for GFP and AV. Cells were treated with AV-binding buffer without (None) (Control (b), n=17; + amiloride (d), n=8) or with 1 μ M A23187 (Control (b), n=15; + amiloride (d), n=21). e Representative bright-field images of cells expressing TMEM16E WT or E584Q treated AV-binding buffer without or with 1 μ M A23187. Images at 0' and 15'

after application of AV-binding buffer without or with amiloride. The black dashed square boxes are magnified in the 0' and 15' images in the bottom panel. Scale bars, 10 μ m, and magnified images scale bar, 2 μ m. f Percentage of bleb-positive cells expressing TMEM16E WT or E584Q. Gray bars; None, n=6; +1 μ M A23187, n=5 for TMEM16E WT; None, n=5 for E584Q. Purple bars; None, n=6; +1 μ M A23187, n=6 for TMEM16E WT; None, n=8 for E584Q. Analyzed by two-way ANOVA followed by Tukey's post-hoc test (Compared to TMEM16E WT None control, WT None amiloride, ns > 0.9999; WT 1 μ M A23187 control, ****P < 0.0001; WT 1 μ M A23187 amiloride, ****P < 0.0001; Data are mean \pm SEM.

sensory processing, motor learning, and cognition^{48,49}. Their survival and functionality are essential for cerebellar operations, particularly for movement precision and coordination^{50,51}. We discovered that TMEM16E scramblase activity was induced by 30 mM KCl depolarization (Fig. 7f, g), suggesting that scramblase activation under physiological conditions may support cerebellar function.

In summary, our findings elucidate the protective role of TMEM16E scramblase through macropinocytosis, as demonstrated in both mammalian cell lines and primary neurons. Membrane lipid asymmetry is essential for cellular processes such as trafficking and maintenance of integrity. Scramblase activity can disrupt this asymmetry by redistributing lipids in a calcium-dependent manner⁵². Our work documented that TMEM16E-dependent macropinocytosis emerges as a mechanism for restoring membrane integrity and promoting cell survival. The elucidated molecular pathway of TMEM16E scramblase highlights how PS translocation serves as a cellular "repair signal," suggesting potential therapeutic strategies for muscular dystrophy.

Methods

Cell culture and transfection

HEK293T (large T-antigen transformed HEK293 cells) were cultured in Dulbecco's modified Eagle's medium (DMEM, HyClone; Thermo Fisher Scientific) with 10% fetal bovine serum (HyClone; Thermo Fisher Scientific) and 0.2% penicillin/streptomycin (HyClone; Thermo Fisher Scientific) under standard growth conditions (37 °C and 5% CO₂). HEK293T was transiently transfected using the TransIT-X2 Dynamic Delivery System (MIRUS) according to the manufacturer's protocol. Cells were transfected with 50 ng of GFP-C1, 1000 ng of human TMEM16E-GFP, 1000 ng of human TMEM16E-GFP E584Q, 1000 ng of M₁R, 50 ng of Ds-red, 100 ng of PH-Btk-GFP, or 100 ng of Lyn-mCherry (Lyn-mCh) in a 35 mm cell culture dish at 50% to 60% confluency. For the rapamycin-inducible dimerization system, cells were co-transfected with 300 ng of Lyn11-FRB (LDR), translocatable enzymes (RF-Dead, RF-Sac1, and RF-PJ), and PH-PLCδ1-GFP. Transfected cells were plated on poly-L-lysine coated coverslip chips and used for live-cell imaging and voltage-clamp experiments 48 hours after transfection.

Plasmids and chemicals

Human cDNA clones of TMEM16E (GenBank accession no. NM_001410964.1) were generously given by Anna Boccaccio (Institute of Biophysics, Rome, Italy). Human cDNA clones of TMEM16F (GenBank accession no.NM_001025356.3) were generously provided by Joo Hyun Nam (Dongguk University College of Medicine, Gyeongju, Republic of Korea). The mouse M₁R (GenBank accession no. NM_001112697) from N.N. Nathanson (University of Washington, Seattle, WA). The rapamycininducible dimerization system, RF-Dead, RF-Sac1, RF-INPP5E, RF- PJ, and LDR were provided by Takanari Inoue (Johns Hopkins University, Baltimore, MD, USA) and Gerald R. Hammond (University of Pittsburgh School of Medicine, Pittsburgh, PA, USA). The PH(PLCδ1)-GFP was provided by Bertil Hille (University of Washington School of Medicine, Seattle, WA, USA). The PH-Btk-GFP originating from Tamas Balla (Institute of Child Health and Human Development, Bethesda, MD, USA). The mCherry-N1

vectors from Clontech. The following chemicals were obtained: Amiloride hydrochloride (Tocris); 10,000 MW dextran, Alexa Fluor 680 (Invitrogen); FITC-Dextran 70,000 MW (Sigma-Aldrich); afatinib (BIBW 2992, Selleckchem); imatinib (STI571, Selleckchem); wortmannin (Enzo); IPA-3 and EHT-1864 (MCE); oxotremorine-M (Oxo-M; Research Biochemicals), and other chemicals (Sigma-Aldrich).

Molecular cloning

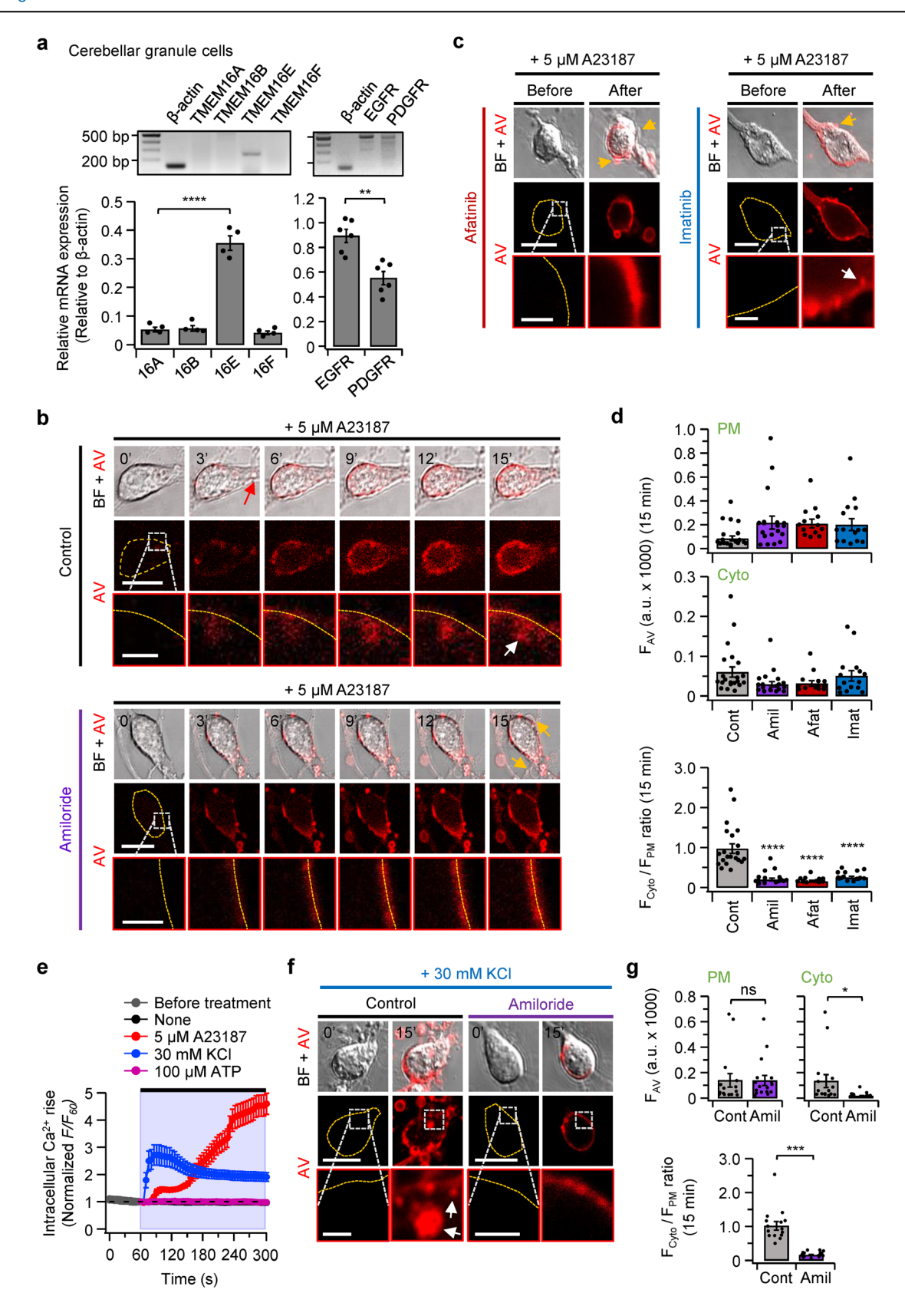
Human cDNAs of EGFR (Plasmid #133749) and PDGFR (Plasmid #136455) were purchased from Addgene, and coding regions were subcloned into a pcDNA 3.1(+) vector. The cDNAs encoding EGFR and PDGFR were amplified by PCR using nTenuto DNA polymerase (Enzynomics), and EGFR and PDGFR were TA cloned into T-Easy vector (Promega) and TOPO vector (Invitrogen), respectively. The mutant form was constructed from wild-type hTMEM16E. Deletion, Triple-HA- tag (HAx3) insertion, and single amino acid mutant was generated by the inverse PCR method using pfu Turbo DNA polymerase (Agilent Technologies), plasmid DNA was digested by Dpn I (Enzynomics), the PCR product was 5′-phosphorylated by T4 polynucleotide kinase (Enzynomics) and ligated by T4 DNA ligase (NEB). The mutant form was verified by DNA sequencing (Macrogen).

Confocal microscopy

All images were taken with Carl Zeiss LSM 700 or LSM 800 confocal microscopes (ZEISS) at room temperature (22-25 °C). Cell images were scanned by using a 40X (water) objective lens at 1024 × 1024 pixels using digital zoom. For the time courses, scramblase assay images were taken every 30 s in imaging software (Zen black) at 512 x 512 pixels using digital zoom, and images of the rapamycin-inducible dimerization system were taken every 10 s⁵³. Cells were bathed in an external solution that contained: 140 mM NaCl, 2.5 mM CaCl₂, and 10 mM HEPES, adjusted to pH 7.4 with NaOH. To analyze scrambling activity, regions of interest (ROIs) were selected in the whole plasma membrane, or cytoplasm regions of cells in Zen software (black edition, ZEISS). To analyze colocalization, we calculated the Pearson's correlation coefficient (R2) value using Fiji software and the Colocalization Threshold plugin. A correlation coefficient (R2) value of "1" indicates perfect colocalization, and "0" signifies random (no) colocalization⁵⁴. To monitor the changes in PI(3,4,5)P₃ levels in the plasma membrane, cells were starved for 6 h in DMEM without serum and then transferred to culture medium containing 10% FBS. All images were converted to JPEG format, and raw data from the time course experiments were processed with Microsoft Office Excel 365 and Igor Pro (WaveMetrics).

Scramblase Assay

Scramblase was assessed by live-cell imaging of the binding of Annexin-V conjugated to Alexa Fluor-568 or Alexa Fluor-647 diluted 1:200 (Invitrogen). TMEM16E scramblase activity was induced by elevating intracellular Ca^{2+} levels using the A23187 (Sigma-Aldrich), a Ca^{2+} ionophore. In most of these experiments, cells were incubated for 15 min in 1 μ M A23187, AV (diluted 1:200), and 2.5 mM Ca^{2+} concentration. In some experiments with M1R-transfected cells, the scramblase was induced by treatment with 10 μ M Oxo-M. To evoke endogenous Ca^{2+} -PLS, cells



were preincubated with Zero Ca $^{2+}$ and 10 μM A23187 for 5 min, and then 2.5 mM Ca $^{2+}$ and Annexin-V diluted 1:200 for 15 min, the 10° protocol. The scrambling activity was recorded by time-lapse imaging for 15 min with a 30 s acquisition interval.

Cell Lysis and Co-immunoprecipitation

HEK293T cells were seeded on a 100-mm cell culture dish (Falcon) in a cell culture medium at 50% to 60% confluency. The next day, cells were starved for 4 hours in DMEM and then transfected with $10~\mu g$ of TMEM16E-GFP,

Fig. 7 | Expression of TMEM16 family, lipid scrambling, and macropinocytosis in primary- cultured granule cells. a Expression of mRNA for different TMEM16E family members (n = 4) and receptor tyrosine kinases (n = 6) in cerebellar granule cells (7-9 days in vitro) from P5 to P6 Sprague-Dawley rats using RT-PCR. mRNA expression levels were normalized relative to β-actin. Analysis was performed by one-way ANOVA followed by Dunnett's post-hoc test (****P < 0.0001) and determined by Student's t-test (**P = 0.0011). **b**, **c** Representative images of 5 μ M A23187- induced scrambling activity of endogenous scramblases in primarycultured granule cells representing control or application of 3 mM amiloride for 15 min (b), and pretreated with 1 μ M afatinib or 20 μ M imatinib for 1 h (c). Inhibitor treatments preceded imaging in the neurobasal medium. The yellow dashed lines represent the plasma membrane area and the white dashed square box is magnified in the images in the bottom panel. The red arrow indicates cytoskeletal remodeling at the plasma membrane, the white arrow internalized AVs, and the yellow arrows membrane blebbing. Scale bars, 10 μm and magnified images scale bar, 2 μm. d Effect of inhibitors on AV fluorescence intensity at 15 min after induction of scramblase (Control, n = 21; Amiloride, n = 19; Afatinib, n = 13; Imatinib, n = 15). ROIs selected plasma membrane (PM) and cytoplasmic regions (Cyto). The intensity ratio of the cytoplasmic region to the plasma membrane (F_{Cyto}/F_{PM} ratio) is shown below.

****P < 0.0001. Analysis performed by one-way ANOVA followed by Dunnett's post-hoc test. e Time course of intracellular Ca2+ (fluo-4 fluorescence) measured every 5 s (None, n = 39; 5 μ M A23187, n = 34; 30 mM KCl, n = 41; 100 μ M ATP, n = 25) in granule cells. Cells were treated with Fluo-4-AM for 10 min in Ringer's solution containing 2.5 mM Ca²⁺ before imaging. The gray circle represents the Fluo-4-AM fluorescence intensity in Ringer's solution. Cytoplasmic fluorescence intensities were normalized relative to F₆₀. f Representative images of 30 mM KClinduced scrambling activity of endogenous scramblases in primary-cultured granule cells represent control and application of 3 mM amiloride for 15 min in neurobasal medium. The yellow dashed lines represent the plasma membrane area and the white dashed square box is magnified in the bottom panel images. The white arrow represents internalized AVs. Scale bars, $10 \, \mu m$ and magnified images scale bar, $2 \, \mu m$. g Analysis of AV fluorescence intensity during 30 mM KCl-induced scrambling activity in granule cells (Control, n = 15; Amiloride, n = 17). Granule cells were treated with 3 mM amiloride for 15 min in neurobasal medium before imaging. ROIs were selected plasma membrane (PM), and cytoplasmic region (Cyto). The ratio of the cytoplasmic region to the plasma membrane is plotted. Compared with control, determined by Student's t-test (PM, ns = 0.9823; Cyto, *P = 0.0412; F_{Cyto}/F_{PM} ratio, ***P < 0.001). Data are mean \pm SEM.

4 μg of PDGFR-HAx3, 4 μg of EGFR HAx3, and 8 μg HAx3 M1R using TransIT-X2 Dynamic Delivery System (MIRUS). After 6 hours, DMEM was replaced with a cell culture medium. Next, cell lysates were prepared in co-immunoprecipitation lysis buffer: 50 mM Tris-HCl (pH 8.0) (Duchefa Biochemie), 1 mM EDTA (Calbiochem), 50 mM NaCl (Sigma-Aldrich), 1% TritonX-100 (Sigma-Aldrich), 10% glycerol (Duchefa Biochemie)) supplemented with 1 mM phenylmethylsulfonyl fluoride (PMSF, Sigma-Aldrich), 1x Halt protease & phosphatase inhibitor cocktail (Thermo Fisher Scientific). Cell lysates were vortexed and incubated three times for 10 min at 4 °C and centrifuged at 132,000 rpm for 15 min. Protein quantification was performed using a Pierce BCA protein assay kit (Thermo Fisher Scientific). To prepare immune complexes, protein lysates 2 mg were mixed with 2 µg rabbit-anti HA or control rabbit IgG (R&D systems) antibody and rotated overnight using a rotator at 4 °C. Immune complexes were collected by incubation with Protein G-magnetic beads (Bio-Rad) or Protein A/G-PLUS Agarose beads (Santacruz) at 4 °C with agitation for 6 h. The immune complexes bound to magnetic beads were spun down and washed using magnetic beads (Thermo Fisher Scientific) three times with wash buffer (50 mM Tris-HCl (pH 8.0), 1 mM EDTA, 250 mM NaCl, 1% TritonX-100, 10% glycerol). The protein complexes were mixed with 40 µL coimmunoprecipitation lysis buffer and 10 µL sample buffer (Mentos) containing 250 mM Tris-HCl (pH 6.8), 0.5 M DTT, 10% SDS, 50% Glycerol, and 0.2% Bromophenol blue and denatured at 37 °C for 30 min using a heating shaker incubator (Thermo Fisher Scientific).

Western blotting

For western blot analysis, co-immunoprecipitation samples and 5% input samples were loaded on 8% SDS-PAGE and electrophoresed at 74 V for 30 min and at 130 V for 90 min. After electrophoresis, proteins were transferred to the PVDF membrane (Millipore) for 30 min at 25 V, and the PVDF membrane was incubated in a blocking buffer containing 5% skim milk powder (Sigma-Aldrich) and 1x TBS-T at room temperature for 1 hour. Next, the PVDF membrane was washed three times with 10 mL 1x TBS-T. The membrane was treated with primary antibody (mouse anti-GFP 1:100, Santacruz sc-9996; mouse anti-HA 1:200, Santacruz sc-7392; rabbit anti- GAPDH 1:25,000, and Cell signaling technology #2955) supplemented with 3% BSA (MP Biomedicals) in 1x TBS-T for overnight at 4°C and washed three times with 10 mL 1x TBS-T. After the primary antibody was removed, the membrane was incubated with secondary antibody (anti-mouse IgG 1:10,000, Thermo Fisher Scientific; anti-rabbit IgG 1:10,000, Thermo Fisher Scientific) in 5% blocking buffer at room temperature for 1 hour and washed three times. Western blots were developed with electrochemiluminescence solutions (Thermo Fisher Scientific) and signals were collected with X-ray film. Images were analyzed using Image J software.

Reverse transcription-PCR

Total RNA was extracted from the HEK293T cells or granule cells cultured from Sprague-Dawley rats aged P5-P6, using RNase desaturating solution (Promega) or QIAzol Lysis Reagent (QIZHEN) and 2 M sodium acetate. Reverse transcription reactions were conducted with the TOPscript cDNA Synthesis kit (Enzynomics) according to the manufacturer's instructions. Expression of the target gene was normalized to the housekeeping gene β -actin. All images were analyzed by Image J software.

Dissection and dissociation of primary granule cells

Granule cells were cultured from Sprague-Dawley rats aged P5 to P6 regardless of gender. The cerebellum of rats euthanized quickly by decapitation was removed by dissection. The meninges were carefully removed from the cerebellum and the cerebellum gently washed with 10 mL Hanks's balanced salt solution (HBSS, Gibco) without Ca²⁺ and Mg²⁺ in a 15 mL conical tube (Falcon). Next, the dissected cerebellum was incubated in 5 mL HBSS and 0.025% trypsin (Gibco) for 15 min with inversion every 2–3 min. After incubation and digestion with the enzymes, the cerebellum was washed twice in the plating medium: basal medium eagle (BME; Gibco) with 10% FBS, 20% glucose (Merck), 200 mM glutamine (Gibco), and penicillin/ streptomycin. To obtain granule cells, the cerebellum was partially dissociated by gentle pipetting with 4 mL plating medium and then filtered using a wetted cell strainer (40 µm mesh, Falcon) into a 50 mL conical tube (Falcon). Granule cells were transferred to a new 15 mL conical tube and 4 mL of plating medium added, then centrifuged at 200 g for 2 min. Finally, the supernatant was aspirated, and isolated granule cells were resuspended in the granule cell growth medium containing: neurobasal medium (Gibco) supplemented with 2% B27 (Gibco), 20 mM KCl (Gibco), 2 mM glutamine (Sigma-Aldrich), and 1% penicillin/streptomycin⁵⁵. The granule cells were seeded at a density of 1.5 x 105 cells/well on Poly-L-lysine coated glass coverslips in 12-well plates (Falcon), and 4.0 x 10⁵ cells/well in a 35 mm confocal chamber (SPL). The next day, 10 µM cytosine beta-D- arabinofuranoside was added (Ara-C, Sigma-Aldrich) to inhibit the division of microglia and astrocytes⁵⁶. For sustaining neuronal growth, half of the medium was replaced with fresh granule cell growth medium twice a week. All the animal experiments were performed according to the ethical guidelines of the Laboratory Animal Resource Center, DGIST (LARC DGIST) approved. We have complied with all relevant ethical regulations for animal use.

Electrophysiological recordings

TMEM16E current recording was performed in the whole-cell voltageclamp configuration at room temperature (22 to 25 °C) using a HEKA EPC-10 amplifier with Pulse software (HEKA Elektronik). Electrode pipettes pulled from glass micropipette capillaries (Sutter Instrument) had

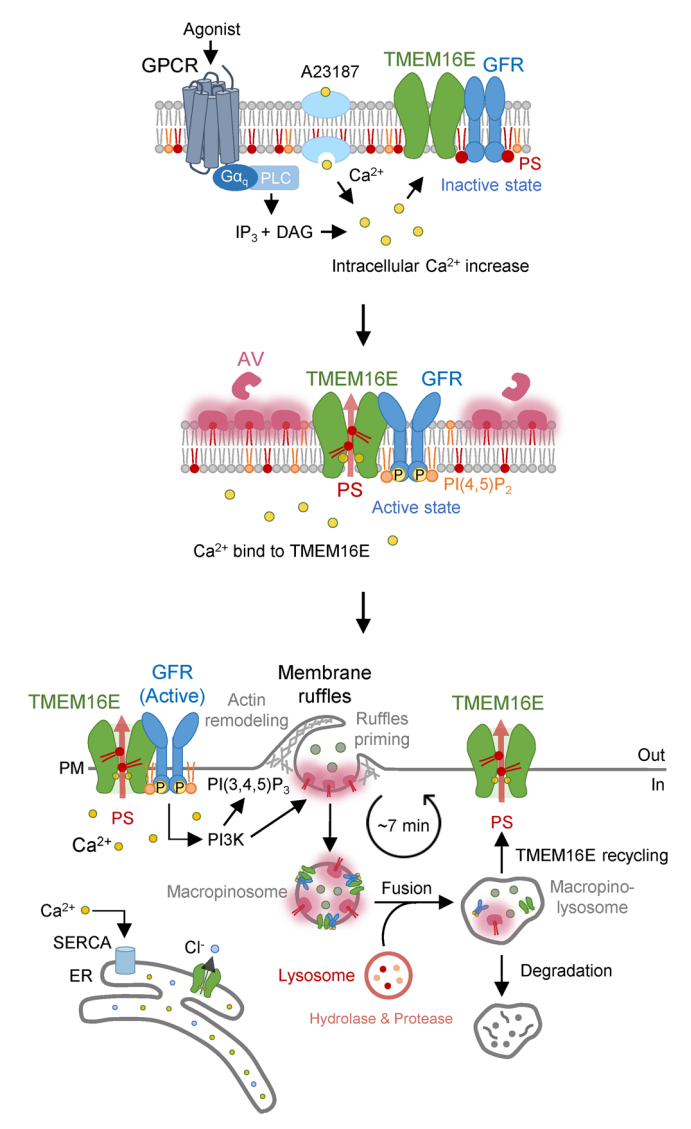


Fig. 8 | Proposed mechanism of TMEM16E-dependent macropinocytosis. TMEM16E-dependent scramblase is activated by 1 μ M A23187 or 10 μ M Oxo-M in cells expressing TMEM16E or co-expressing M1R and TMEM16E. Application of 1 μ M A23187 allows extracellular Ca^{2+} to enter cells, and application of 10 μ M Oxo-M activates M_1R , and Ca^{2+} release from the ER. Increased intracellular Ca^{2+} binds to TMEM16E, activating scramblase activity. The scramblase translocates PS from the inner leaflet to the outer leaflet, where it binds to AVs. $PI(4,5)P_2$ clustered at TMEM16E interacts with and activates GFR, resulting in P13K activation and synthesis of $PI(3,4,5)P_3$. Increased $PI(3,4,5)P_3$ induces membrane ruffling and priming to form macropinosomes. Macropinosomes fuse with lysosomes; AVs and GFRs are degraded through the lysosomal degradation pathway, and TMEM16E is recycled into the plasma membrane. In addition, intracellular calcium is regulated by TMEM16E and SERCA pumps located in the ER. The images and every material element by the authors using Microsoft Office PowerPoint 365 (Microsoft).

resistances of 2–4 M Ω , and series-resistance errors were compensated by 60%. TMEM16E currents were recorded with a membrane holding potential of –60 mV and applying a 500 ms test pulse. All current data were analyzed using Igor Pro 6.0 (WaveMetrics). The external Ringer's solution consisted of 150 mM NaCl, 1 mM CaCl₂, 1 mM MgCl₂, 10 mM Glucose, and 10 mM HEPES, pH was adjusted to pH 7.4 with NaOH. The Zero Ca²⁺ internal pipette solution contained 130 mM CsCl, 1 mM MgCl₂, 10 mM EGTA, 3 mM Na₂ATP, and 10 mM HEPES, pH was adjusted to pH 7.35 with CsOH. For 3 μ M free Ca²⁺ pipette solution, added CaCl₂ was 4.7 mM and the Ca2+ chelator was replaced by 10 mM HEDTA-Na3. (Free Ca2+

calculated with the Ca²⁺/Mg²⁺/ATP/EGTA/HEDTA calculator, version 2.2b, available at https://somapp.ucdmc.ucdavis.edu/pharmacology/bers/maxchelator/webmaxc/webmaxcS.htm).

Ca²⁺ imaging

For measuring intracellular Ca^{2+} levels, transfected cells on coverslips were pre-incubated with 2.5 mM Ca^{2+} Ringer's solutions containing 4 μ M of Fluo-4 AM (Invitrogen) for 10 min at 37 °C and 5% CO_2^{57} . Time-course experiments of cytoplasmic fluorescence intensity were imaged at 512 \times 512 pixels every 5 s. For measuring the intracellular Ca^{2+} influx, regions of interest (ROIs) were selected in the cytoplasm region of cells in Zen software (black edition, ZEISS).

Optical microscopy

Bright-field and total internal reflection fluorescence (TIRF) microscopy were performed under the inverted microscope (Nikon, ECLIPSE Ti2-E) equipped with a motorized stage (Ti2-S-SE-E), a perfect focus system (PFS, Ti2-N-ND-P), a fluorescence filter cube (Quad filter set 405/488/561/640 nm), and an electron-multiplying charge-coupled device (EM CCD, Andor, iXon Ultra 897). A temperature and CO₂-concentration controlled stage-top-incubator (Okolab, UNO- T-H-PREMIXED) was used for live cell imaging. LED lamp (Nikon, Ti2-D-LHLED) and laser (Nikon, LU-N4 Laser Unit, 488/561 nm for observing GFP/Alexa 568) were taken as a light source for bright field and TIRF, respectively. The H-TIRF module (Nikon, TI-LA-HTIRF) was used to automatically adjust the penetration depth of the evanescent wave to 250 nm. All images were acquired with a 100x objective lens (Nikon, 1.49 NA, oil immersion, CFI SR HP Apochromat TIRF).

Lentivirus transduction

GFP were subcloned into a pLenti-III-mir-GFP-Blank-abmgood_m001 (Abmgood), and TMEM16E-GFP was subcloned into a pEz-Lv-CMV-N-3xHA-Nurr1 (Genecopoeia). Hxadimethrine bromide (Polybrene) were purchased from Sigma-Aldrich (#H9268). Plasmids were transiently expressed in HEK293T cells using TransIT-X2 reagent (MIRUS). For lentiviral transduction, HEK293T cells were treated with viral supernatants and 8 μ g/mL polybrene to cell culture medium in 12-well plates at 70% confluency. To select for stable expression of the transgene, cells were treated with 1 μ g/mL puromycin.

TMEM16E knockdown by shRNA in primary-cultured rat cerebellar granule cells

shRNA constructs targeting TMEM16E were cloned into U6-(shRNA)-hSyn-EGFP vectors, derived from pAAV-U6-sgRNA-CMV-GFP (Addgene, #85451) and pAAV-hSyn-EGFP (Addgene, #50465). Four distinct shRNA sequences were utilized to induce RNA interference (RNAi). The target sequences within rat TMEM16E and the sequences of the shRNA oligonucleotides are listed in Supplementary Table 1. Knockdown in primary-cultured rat cerebellar granule cells from Sprague-Dawley rats aged P5 to P6 was achieved by transfecting the shRNA constructs using Lipofectamine 2000 (Invitrogen) or TransIT-X2 reagent (Mirus).

Statistics and reproducibility

Data were analyzed using Microsoft Office Excel 365 (Microsoft), Igor Pro 6.0 (WaveMetrics), Zen software (black edition, ZEISS), Image J-Fiji software (NIH), or GraphPad Prism 7.02 (GraphPad Software). Statistics in text or figures represent mean \pm SEM. Statistical comparisons between two groups were analyzed using Student's t-test. The significance of observations across multiple groups was assessed using one-way ANOVA or two-way ANOVA followed by Sidak's, Dunnett's, and Tukey's post-hoc test. Differences were considered significant at the $^*P < 0.05, \ ^{**}P < 0.01$, and $^{***}P < 0.001$ levels. Each experiment was repeated at least 3 times independently.

Reporting summary

Further information on research design is available in the Nature Portfolio Reporting Summary linked to this article.

Data availability

The source data behind the graphs in the paper can be found in Supplementary Data 1. Uncropped western blots and gel images are included in the Supplementary information. All other data supporting the findings of this study are available from the corresponding author upon request.

Received: 28 March 2024; Accepted: 3 January 2025; Published online: 10 January 2025

References

- Di Zanni, E., Gradogna, A., Scholz-Starke, J. & Boccaccio, A. Gain of function of TMEM16E/ANO5 scrambling activity caused by a mutation associated with gnathodiaphyseal dysplasia. *Cell. Mol. Life* Sci. 75, 1657–1670 (2018).
- Whitlock, J. M., Yu, K., Cui, Y. Y. & Hartzell, H. C. Anoctamin 5/ TMEM16E facilitates muscle precursor cell fusion. *J. Gen. Physiol.* 150, 1498–1509 (2018).
- Le, T. et al. An inner activation gate controls TMEM16F phospholipid scrambling. Nat. Commun. 10, 1846 (2019).
- Malvezzi, M. et al. Out-of-the-groove transport of lipids by TMEM16 and GPCR scramblases. Proc. Natl Acad. Sci. USA 115, E7033–E7042 (2018).
- Falzone, M. E. et al. TMEM16 scramblases thin the membrane to enable lipid scrambling. *Nat. Commun.* 13, 2604 (2022).
- Ma, X. et al. Phosphatidylserine, inflammation, and central nervous system diseases. Front. Aging Neurosci. 14, 975176 (2022).
- Suzuki, J. et al. Calcium-dependent phospholipid scramblase activity of TMEM16 protein family members. J. Biol. Chem. 288, 13305–13316 (2013).
- Lee, S. H., Meng, X. W., Flatten, K. S., Loegering, D. A. & Kaufmann, S. H. Phosphatidylserine exposure during apoptosis reflects bidirectional trafficking between plasma membrane and cytoplasm. Cell Death. Differ. 20, 64–76 (2013).
- Andrews, N. W. & Corrotte, M. Plasma membrane repair. Curr. Biol. 28, R392–R397 (2018).
- Recouvreux, M. V. & Commisso, C. Macropinocytosis: A metabolic adaptation to nutrient stress in cancer. Front. Endocrinol. (Lausanne) 8, 261 (2017).
- Falcone, S. et al. Macropinocytosis: Regulated coordination of endocytic and exocytic membrane traffic events. *J. Cell Sci.* 119, 4758–4769 (2006).
- Wu, N. et al. Critical role of lipid scramblase TMEM16F in phosphatidylserine exposure and repair of plasma membrane after pore formation. *Cell Rep.* 30, 1129–1140 (2020).
- Foltz, S. J., Cui, Y. Y., Choo, H. J. & Hartzell, H. C. ANO5 ensures trafficking of annexins in wounded myofibers. *J. Cell Biol.* 220, e202007059 (2021).
- Chandra, G. et al. Dysregulated calcium homeostasis prevents plasma membrane repair in Anoctamin 5/TMEM16E-deficient patient muscle cells. Cell Death Discov. 5, 118 (2019).
- Koivusalo, M. et al. Amiloride inhibits macropinocytosis by lowering submembranous pH and preventing Rac1 and Cdc42 signaling. *J. Cell Biol.* 188, 547–563 (2010).
- Kodigepalli, K. M., Bowers, K., Sharp, A. & Nanjundan, M. Roles and regulation of phospholipid scramblases. FEBS Lett. 589, 3–14 (2015).
- Chen, Z. et al. Characterizing the binding of annexin V to a lipid bilayer using molecular dynamics simulations. Proteins 82, 312–322 (2014).
- Yeung, T. et al. Membrane phosphatidylserine regulates surface charge and protein localization. Science 319, 210–213 (2008).
- 19. Yeung, T. et al. Contribution of phosphatidylserine to membrane surface charge and protein targeting during phagosome maturation. *J. Cell Biol.* **185**, 917–928 (2009).

- Doherty, G. J. & McMahon, H. T. Mechanisms of endocytosis. *Annu. Rev. Biochem.* 78, 857–902 (2009).
- Sønder, S. L. et al. Restructuring of the plasma membrane upon damage by LC3-associated macropinocytosis. Sci. Adv. 7, eabg1969 (2021).
- Cruz-Rangel, S. et al. Extracellular protons enable activation of the calcium-dependent chloride channel TMEM16A: Tuning TMEM16A activation with external protons. *J. Physiol.* 595, 1515–1531 (2017).
- Di Zanni, E., Gradogna, A., Picco, C., Scholz-Starke, J. & Boccaccio, A. TMEM16E/ANO5 mutations related to bone dysplasia or muscular dystrophy cause opposite effects on lipid scrambling. *Hum. Mutat.* 41, 1157–1170 (2020).
- Jun, I. et al. ANO9/TMEM16J promotes tumourigenesis via EGFR and is a novel therapeutic target for pancreatic cancer. *Br. J. Cancer* 117, 1798–1809 (2017).
- Bill, A. et al. ANO1/TMEM16A interacts with EGFR and correlates with sensitivity to EGFR- targeting therapy in head and neck cancer. Oncotarget 6, 9173–9188 (2015).
- Kurokawa, K., Itoh, R. E., Yoshizaki, H., Nakamura, Y. O. T. & Matsuda, M. Coactivation of Rac1 and Cdc42 at lamellipodia and membrane ruffles induced by epidermal growth factor. *Mol. Biol. Cell* 15, 1003–1010 (2004).
- Lee, S. W. et al. EGFR-Pak signaling selectively regulates glutamine deprivation-induced macropinocytosis. *Dev. Cell* 50, 381–392 (2019).
- Schmees, C. et al. Macropinocytosis of the PDGF β-receptor promotes fibroblast transformation by H-Ras(G12V). Mol. Biol. Cell 23, 2571–2582 (2012).
- Barker, S. A., Caldwell, K. K., Pfeiffer, J. R. & Wilson, B. S. Wortmannin-sensitive phosphorylation, translocation, and activation of PLCγ1, but not PLCγ2, in antigen-stimulated RBL-2H3 mast cells. *Mol. Biol. Cell* 9, 483–496 (1998).
- Yoshida, S., Hoppe, A. D., Araki, N. & Swanson, J. A. Sequential signaling in plasma- membrane domains during macropinosome formation in macrophages. J. Cell Sci. 122, 3250–3261 (2009).
- Suh, B. C., Inoue, T., Meyer, T. & Hille, B. Rapid chemically induced changes of PtdIns(4,5)P2 gate KCNQ ion channels. *Science* 314, 1454–1457 (2006).
- 32. Quinn, S. E. et al. The structural dynamics of macropinosome formation and Pl3-kinase- mediated sealing revealed by lattice light sheet microscopy. *Nat. Commun.* **12**, 4838 (2021).
- Kim, D. H., Triet, H. M. & Ryu, S. H. Regulation of EGFR activation and signaling by lipids on the plasma membrane. *Prog. Lipid Res.* 83, 101115 (2021).
- 34. Hammond, G. R. V. et al. PI4P and PI(4,5)P2 are essential but independent lipid determinants of membrane identity. *Science* **337**, 727–730 (2012).
- 35. Cohen, P., Cross, D. & Jänne, P. A. Kinase drug discovery 20 years after imatinib: progress and future directions. *Nat. Rev. Drug Discov.* **20**, 551–569 (2021).
- Malavaki, C. J. et al. Imatinib as a key inhibitor of the platelet-derived growth factor receptor mediated expression of cell surface heparan sulfate proteoglycans and functional properties of breast cancer cells. FEBS J. 280, 2477–2489 (2013).
- Zhang, W., Schmelzeisen, S., Parthier, D., Frings, S. & Möhrlen, F. Anoctamin calcium- activated chloride channels may modulate inhibitory transmission in the cerebellar cortex. *PLoS One* 10, e0142160 (2015).
- Keefe, D. et al. Perforin triggers a plasma membrane-repair response that facilitates CTL induction of apoptosis. *Immunity* 23, 249–262 (2005).
- 39. Kulma, M. & Anderluh, G. Beyond pore formation: reorganization of the plasma membrane induced by pore-forming proteins. *Cell. Mol. Life Sci.* **78**, 6229–6249 (2021).
- Idone, V. et al. Repair of injured plasma membrane by rapid Ca²⁺dependent endocytosis. *J. Cell Biol.* 180, 905–914 (2008).

- 41. Cooper, S. T. & McNeil, P. L. Membrane repair: mechanisms and pathophysiology. *Physiol. Rev.* **95**, 1205–1240 (2015).
- Dias, C. & Nylandsted, J. Plasma membrane integrity in health and disease: significance and therapeutic potential. Cell Discov. 7, 1–18 (2021).
- Merregaert, J. et al. Phospholipid scramblase 1 is secreted by a lipid raft-dependent pathway and interacts with the extracellular matrix protein 1 in the dermal epidermal junction zone of human skin. *J. Biol. Chem.* 285, 37823–37837 (2010).
- Sun, J., Nanjundan, M., Pike, L., Wiedmer, T. & Sims, P. Plasma membrane phospholipid scramblase 1 is enriched in lipid rafts and interacts with the epidermal growth factor receptor. *Biochemistry* 41, 6338–6345 (2002).
- Lambert, S., Vind-Kezunovic, D., Karvinen, S. & Gniadecki, R. Ligandindependent activation of the EGFR by lipid raft disruption. *J. Invest. Dermatol.* 126, 954–962 (2006).
- Henriksen, L., Grandal, M. V., Knudsen, S. L. J., van Deurs, B. & Grøvdal, L. M. Internalization mechanisms of the epidermal growth factor receptor after activation with different ligands. *PLoS One* 8, e58148 (2013).
- Xu, J. et al. A novel ANO5 splicing variant in a LGMD2L patient leads to production of a truncated aggregation-prone Ano5 peptide. *J. Pathol. Clin. Res.* 4, 135–145 (2018).
- Consalez, G. G., Goldowitz, D., Casoni, F. & Hawkes, R. Origins, development, and compartmentation of the granule cells of the cerebellum. Front. Neural Circuits 14, 611841 (2021).
- Koziol, L. F. et al. Consensus paper: The cerebellum's role in movement and cognition. Cerebellum 13, 151–177 (2014).
- Galliano, E. et al. Silencing the majority of cerebellar granule cells uncovers their essential role in motor learning and consolidation. *Cell Rep.* 3, 1239–1251 (2013).
- 51. Badura, A. & De Zeeuw, C. I. Cerebellar granule cells: dense, rich and evolving representations. *Curr. Biol.* **27**, R415–R418 (2017).
- Fadeel, B. & Xue, D. The ins and outs of phospholipid asymmetry in the plasma membrane: Roles in health and disease. *Crit. Rev. Biochem. Mol. Biol.* 44, 264–277 (2009).
- Ko, W. & Suh, B. C. Differential regulation of Ca²⁺-activated Cl⁻channel TMEM16A splice variants by membrane PI(4,5)P2. Int. J. Mol. Sci. 22, 4088 (2021).
- 54. Ko, W. et al. Allosteric modulation of alternatively spliced Ca²⁺-activated Cl⁻ channels TMEM16A by PI(4,5)P2 and CaMKII. *Proc. Natl Acad. Sci. USA* **117**, 30787–30798 (2020).
- Brewer, G. J. Serum-free B27/neurobasal medium supports differentiated growth of neurons from the striatum, substantia nigra, septum, cerebral cortex, cerebellum, and dentate gyrus. *J. Neurosci.* Res. 42, 674–683 (1995).
- Tehran, D. A. & Pirazzini, M. Preparation of cerebellum granule neurons from mouse or rat pups and evaluation of clostridial neurotoxin activity and their inhibitors by Western blot and immunohistochemistry. *Bio. Protoc.* 8, e2918 (2018).
- 57. Kim, D. I., Kweon, H. J., Park, Y., Jang, D. J. & Suh, B. C. Ca^{2+} controls gating of voltage- gated calcium channels by releasing the β 2e subunit from the plasma membrane. *Sci. Signal.* **9**, ra67 (2016).

Acknowledgements

We thank the laboratories that kindly provided plasmids. This research was supported by a grant from the National Research Foundation of Korea (NRF)

funded by the Ministry of Science, Information and Communications Technology, and Future Planning (RS-2024-00351000).

Author contributions

J.-E.K., W.K., B.H., and B.-C.S. designed and interpreted the study; J.-E.K. performed all experiments and analyzed data unless otherwise indicated; J.-E.K., S.J. and D.S. conceptualized the TIRF microscopy study. J.-E.K. and S.J. performed TIRF microscopy; J.-N.W. designed the primary-cultured granule cells protocol and TMEM16E KD by shRNA in granule cells; J.-E.K. and J.-N.W. prepared primary-cultured granule cells; J.-E.K and I.B constructed a mutant of TMEM16E; J.-E.K., Y.J. and H.-K.C. designed the lentiviral transduction system; Y.J. subcloned plasmids for lentiviral transduction and prepared viruses. J.-E.K., B.H., and B.-C.S. wrote the manuscript. B.-C.S. supervised the project.

Competing interests

The authors declare no competing interests.

Additional information

Supplementary information The online version contains supplementary material available at https://doi.org/10.1038/s42003-025-07465-6.

Correspondence and requests for materials should be addressed to Byung-Chang Suh.

Peer review information Communications Biology thanks Joachim Scholz-Starke and the other, anonymous, reviewer(s) for their contribution to the peer review of this work. Primary Handling Editors: Dr Lei Zheng and Dr Ophelia Bu.

Reprints and permissions information is available at

http://www.nature.com/reprints

Publisher's note Springer Nature remains neutral with regard to jurisdictional claims in published maps and institutional affiliations.

Open Access This article is licensed under a Creative Commons Attribution-NonCommercial-NoDerivatives 4.0 International License, which permits any non-commercial use, sharing, distribution and reproduction in any medium or format, as long as you give appropriate credit to the original author(s) and the source, provide a link to the Creative Commons licence, and indicate if you modified the licensed material. You do not have permission under this licence to share adapted material derived from this article or parts of it. The images or other third party material in this article are included in the article's Creative Commons licence, unless indicated otherwise in a credit line to the material. If material is not included in the article's Creative Commons licence and your intended use is not permitted by statutory regulation or exceeds the permitted use, you will need to obtain permission directly from the copyright holder. To view a copy of this licence, visit https://creativecommons.org/licenses/by-nc-nd/4.0/.

© The Author(s) 2025